AD-A144 123 HOT ISOSTATIC PRESSING OF CERAMIC POWDER COMPACTS(U) 1/1
BATTELLE COLUMBUS LABS OH J K MCCOY ET AL. 15 JUN 84
AFOSR-TR-84-0617 AFOSR-82-0238

UNCLASSIFIED F/G 11/2 NL

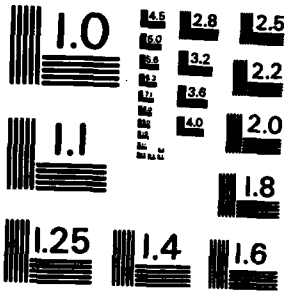

MICROCOPY RESOLUTION TEST CHART
NATIONAL BUREAU OF STANDARDS-1963-A

on

HOT ISOSTATIC PRESSING OF CERAMIC POWDER COMPACTS

(AFOSR CONTRACT 82-0238)
(Project No. 2306/82)

to

THE AIR FORCE OF SCIENTIFIC RESEARCH

SECOND YEAR REPORT

on

HOT ISOSTATIC PRESSING OF CERAMIC POWDER COMPACTS

(AFOSR CONTRACT 82-0238)
(Project No. 2306/82)

to

THE AIR FORCE OF SCIENTIFIC RESEARCH

June 15, 1984

by

R.R. Wills and J.K. McCoy

BATTELLE
Columbus Laboratories
505 King Avenue
Columbus, Ohio 43201

UNCLASSIFIED

SECURITY CLASSIFICATION OF THIS PAGE (When Data Entered)

REPORT DOCUMENTATION PAGE		READ INSTRUCTIONS BEFORE COMPLETING FORM
1. REPORT NUMBER AFOSR-TR- 84-0617	2. GOVT ACCESSION NO. AD-A144 123	3. RECIPIENT'S CATALOG NUMBER
4. TITLE (and Subtitle) Hot Isostatic Pressing of Ceramic Powder Compacts		5. TYPE OF REPORT & PERIOD COVERED 2nd year report: 6/83 - 6/84
		6. PERFORMING ORG. REPORT NUMBER
7. AUTHOR(s) J.K. McCoy and R.R. Wills		8. CONTRACT OR GRANT NUMBER(s) AFOSR 82-0238
9. PERFORMING ORGANIZATION NAME AND ADDRESS Battelle Columbus Laboratories 505 King Avenue, Columbus, Ohio 43201		10. PROGRAM ELEMENT, PROJECT, TASK AREA & WORK UNIT NUMBERS 61102F, 2300/B2
11. CONTROLLING OFFICE NAME AND ADDRESS AFOSR/NE Bolling AFB, D.C. 20332		12. REPORT DATE June 15, 1984
		13. NUMBER OF PAGES
14. MONITORING AGENCY NAME & ADDRESS (if different from Controlling Office)		15. SECURITY CLASS. (of this report) UNCLASSIFIED
		15a. DECLASSIFICATION/DOWNGRADING SCHEDULE

16. DISTRIBUTION STATEMENT (of this Report)

Approved for public release; distribution unlimited.

17. DISTRIBUTION STATEMENT (of the abstract entered in Block 20, if different from Report)

18. SUPPLEMENTARY NOTES

19. KEY WORDS (Continue on reverse side if necessary and identify by block number)

Hot Isostatic Pressing, Alumina, solute diffusion, interface controlled

20. ABSTRACT (Continue on reverse side if necessary and identify by block number)

SUMMARY

The effect of temperature, pressure and time on the rate of densification of submicron alumina powder during hot isostatic pressing has been determined using a dilatometer to continuously monitor volumetric changes. A Fortran computer program is used to make corrections for thermal expansion of the alumina and the stainless steel can, to determine the relative density →

DD FORM 1 JAN 73 1473 EDITION OF 1 NOV 65 IS OBSOLETE

SECURITY CLASSIFICATION OF THIS PAGE (When Data Entered)

of the alumina compact at any point, and to produce report ready graphs depicting the relationship between any two prescribed variables. Analysis of other errors associated with the use of the dilatometer shows that these are negligible compared with thermal expansion effects.

The rate of densification is controlled by an interface reaction mechanism never previously observed in the densification of alumina. Mass transport is limited by the movement of grain boundary dislocations which act as sites for atoms to detach from grains. The actual rate limiting process is the diffusion of solute in the lattice since the motion of solute atoms can result in a large number of atoms being freed from a grain boundary dislocation. Once separated from the dislocation the atoms quickly diffuse away.

Good correlation between experimental data and the theory is given in the relative density range 0.64-0.95, although the theory does not adequately describe pore geometry above 0.9 relative density. The rate of densification in the temperature range 1000-1150°C is given by:

$$\frac{d\,D}{dt} = \frac{3D}{2R}\left(\frac{D}{D_0}\right)^{1/3}\left(\frac{b_n}{b_b}\right)^2 \frac{p^{*2}C_1 D_s \Omega}{G b_b \beta k T C_0}$$

where D = relative density
D_0 = initial relative density
R = particle radius
t = time
b_b = Burgers vector
b_n = component of Burgers reactor normal to the grain boundary
p^* = effective contact stress
C_1 = 0.5
D_s = diffusivity of solute
Ω = effective atomic volume of solute
G = shear modulus
β = ratio of solute concentration near dislocation to solute concentration in bulk
k = Boltzmann's constant
T = temperature
C_0 = bulk solute concentration measured

The measured pressure dependence of 2.1 is also in good agreement with the theoretical prediction of 2. The activation energy was determined to be 290kJ/mole.

TABLE OF CONTENTS

	PAGE
SUMMARY OF DATA AND DATA REDUCTION	1
THEORY OF DENSIFICATION	29
PUBLICATIONS AND PRESENTATIONS	58
ACKNOWLEDGMENTS	58
REFERENCES	59
APPENDIX	60

LIST OF FIGURES

FIGURE 1. HIP PROBE UNIT SHOWING ALUMINA PROBES IN CONTACT WITH STAINLESS STEEL CAN CONTAINING ALUMINA POWDER COMPACT	2
FIGURE 2. DATA FOR EXPERIMENT 14	14
FIGURE 3. DATA FOR EXPERIMENT 19	15
FIGURE 4. DATA FOR EXPERIMENT 20	16
FIGURE 5. DATA FOR EXPERIMENT 21	17
FIGURE 6. DATA FOR EXPERIMENT 22a	18
FIGURE 7. DATA FOR EXPERIMENT 22c	19
FIGURE 8. CROSS SECTION OF HIP CAN AND SAMPLE SHOWING MEASUREMENTS	21
FIGURE 9. GRAIN BOUNDARY DISLOCATION WITH AN ATMOSPHERE OF SOLUTE ATOMS	32
FIGURE 10. GEOMETRY OF TWO SPHERICAL PARTICLES AND A TOROIDAL NECK	35
FIGURE 11. A TWO DIMENSIONAL SCHEMATIC OF A RANDOM PACKING OF SPHERES AND THEIR VORONOI CELLS, AFTER ARZT	37
FIGURE 12. A TYPICAL PARTICLE IN A RANDOM DENSE PACKING AND ITS VORONOI CELL, AFTER ARZT	37

TABLE OF CONTENTS (CONT.)

PAGE

LIST OF FIGURES (CONT.)

FIGURE 13. TWO DESCRIPTIONS OF NECK GEOMETRY. 40

FIGURE 14. CONTRIBUTIONS TO THE EFFECTIVE CONTACT PRESSURE FROM THREE SOURCES AS FUNCTIONS OF DENSITY 42

FIGURE 15. TOTAL EFFECTIVE CONTACT PRESSURE AS A FUNCTION OF DENSITY AT VARIOUS LEVELS OF APPLIED EXTERNAL PRESSURE 44

FIGURE 16. EFFECT OF INITIAL DENSITY ON CALCULATED DENSITY HISTORY. 48

FIGURE 17. COMPARISON BETWEEN EXPERIMENT AND THEORY FOR EXPERIMENT 14 49

FIGURE 18. COMPARISON BETWEEN EXPERIMENT AND THEORY FOR EXPERIMENT 19 50

FIGURE 19. COMPARISON BETWEEN EXPERIMENT AND THEORY FOR EXPERIMENT 20 51

FIGURE 20. COMPARISON BETWEEN EXPERIMENT AND THEORY FOR EXPERIMENT 21 52

FIGURE 21. COMPARISON BETWEEN EXPERIMENT AND THEORY FOR EXPERIMENT 22a. 53

FIGURE 22. COMPARISON BETWEEN EXPERIMENT AND THEORY FOR EXPERIMENT 22c. 54

LIST OF TABLES

TABLE 1. EXPERIMENTAL CONDITIONS FOR HIP EXPERIMENT. 3

TABLE 2. DATA FOR EXPERIMENT 14. 4

TABLE 3. DATA FOR EXPERIMENT 19. 5

TABLE 4. DATA FOR EXPERIMENT 20. 6

TABLE 5. DATA FOR EXPERIMENT 21. 7

TABLE 6. DATA FOR EXPERIMENT 22a 8

TABLE 7. DATA FOR EXPERIMENT 22c 11

TABLE OF CONTENTS (CONT.)

PAGE

LIST OF TABLES (CONT.)

TABLE 8. PHYSICAL MEASUREMENTS OF HIP SAMPLES AND CANS 20

TABLE 9. CAN SIDEWALL VOLUMES AS DETERMINED BY VARIOUS METHODS 26

TABLE 10. COMPARISON OF FINAL DENSITIES AS CALCULATED FROM PROBE DATA AND AS MEASURED BY IMMERSION 27

TABLE 11. GLOSSARY OF TERMS 30

TABLE 12. COMPARISON OF VARIOUS MECHANISMS FOR DENSIFICATION. . . . 56

SUMMARY OF DATA AND DATA REDUCTION

In our HIP experiments, we continuously measure temperature, pressure, and change in can diameter. Changes in can diameter are monitored using two tungsten probes (see Figure 1) which form part of a LVDT circuit. We calculate a continuous record of density as a function of time from these data. As a result, we are able to collect much more information from a single run than is possible in ordinary HIP experiments in which density is recorded only at the beginning and end. In this section all the experimental data is presented. Furthermore, we describe the procedure for converting records of temperature, pressure and can shrinkage into a continuous record of density as a function of time during the HIP experiment. Corrections for thermal expansion together with assumptions regarding the geometry of the sample and can during densification are discussed. A Fortran computer program which carries out these calculations is given in the appendix.

The experiments were planned as one or more periods of time during which the sample was held at roughly constant temperature and pressure. A summary of the conditions for all six experiments is given in Table 1. The experiment numbers in the table will be used throughout this report to distinguish the various runs. In experiments 21, 22a, and 22c, temperature and/or pressure were changed during the experiment so that additional kinetics data could be obtained.

Tables 2 through 7 give values of experimental data. The data were initially recorded on a strip-chart recorder. Values of pressure, temperature, and can shrinkage were read from the charts, correlated with clock time, and keyed into a computer for processing. Temperature was measured at the sample tray, but a simple thermal calculation shows that the temperature at the center of the sample will be largely equilibrated with the temperature at the surface of the can within one minute. "Can shrinkage" is the change in the outside diameter of the can as measured by the probe. Note that the can shrinkage is sometimes negative since thermal expansion is measurable at temperatures too low for densification. The tables also include relative density as calculated

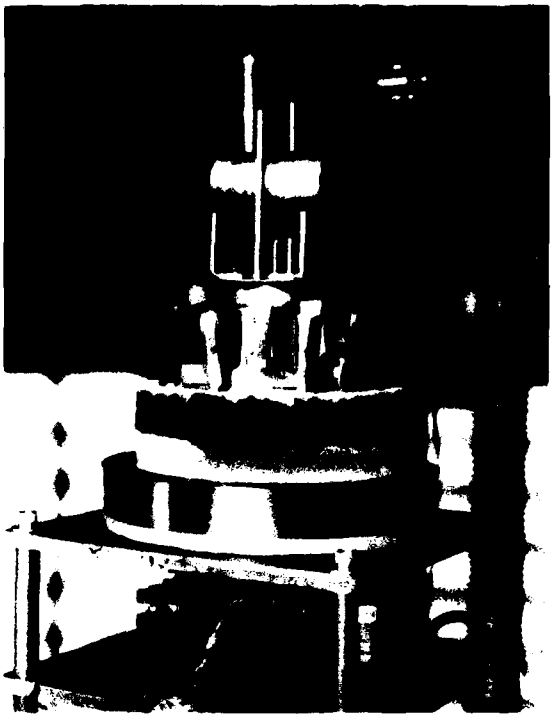

FIGURE 1. HIP PROBE UNIT SHOWING ALUMINA PROBES IN CONTACT WITH STAINLESS STEEL CAN CONTAINING ALUMINA POWDER COMPACT

TABLE 1. EXPERIMENTAL CONDITIONS FOR HIP EXPERIMENTS

Experiment Number	Pressure (MPa)	Temperature (C)
14	101	1150
19	102	1000
20	103	1050
21	34	1000
	70	1000
22a	34	1050
	100	1050
	100	1150
22c	36	1050
	100	1050
	100	1150

TABLE 2. DATA FOR EXPERIMENT 14

Clock time	Elapsed time (min)	Pressure (MPa)	Temperature (C)	Can shrinkage (mm)	Relative density
13:49	0.0	6.9	38	0.000	0.6531
14:02	13.0	20.7	51	0.000	0.6535
14:22	33.0	41.4	67	0.038	0.6583
14:31	42.0	44.1	64	0.044	0.6589
14:47	58.0	73.1	64	0.051	0.6596
14:56	67.0	94.5	65	0.056	0.6602
14:57	68.0	99.3	65	0.056	0.6602
15:40	111.0	93.9	115	-0.013	0.6538
16:40	171.0	98.9	672	-0.176	0.6540
17:06	197.0	99.3	875	-0.184	0.6610
17:20	211.0	99.6	1000	0.260	0.7215
17:26	217.0	100.0	1050	0.657	0.7805
17:33	224.0	100.3	1100	1.086	0.8540
17:39	230.0	100.7	1150	1.467	0.9307
17:50	241.0	100.7	1150	1.586	0.9559
18:09	260.0	100.7	1150	1.594	0.9576

TABLE 3. DATA FOR EXPERIMENT 19

Clock time	Elapsed time (min)	Pressure (MPa)	Temperature (C)	Can shrinkage (mm)	Relative density
12:44	0.0	0.0	29	0.000	0.6536
13:00	16.0	8.3	36	0.000	0.6538
13:05	21.0	16.2	42	0.000	0.6540
13:25	41.0	30.3	58	0.032	0.6581
13:41	57.0	49.0	59	0.040	0.6591
14:08	84.0	102.7	59	0.056	0.6609
15:01	137.0	97.9	285	0.032	0.6653
15:09	145.0	97.9	362	0.000	0.6642
15:18	154.0	98.6	445	-0.032	0.6633
15:27	163.0	98.6	529	-0.063	0.6626
15:52	188.0	99.3	763	-0.127	0.6641
16:13	209.0	100.3	946	-0.127	0.6716
16:19	215.0	100.5	993	0.000	0.6894
16:20	216.0	100.7	1000	0.032	0.6938
16:25	221.0	100.7	1004	0.222	0.7190
16:40	236.0	100.8	1003	0.492	0.7571
16:50	246.0	101.4	1002	0.603	0.7738
17:00	256.0	101.4	1004	0.691	0.7875
17:06	262.0	101.4	1000	0.730	0.7936
17:29	285.0	101.7	1002	0.865	0.8159
17:45	301.0	101.9	1003	0.953	0.8308
18:00	316.0	102.0	1003	1.000	0.8391
18:17	333.0	102.0	1003	1.048	0.8476
18:30	346.0	102.0	1005	1.087	0.8549
18:50	366.0	102.4	1008	1.135	0.8639
18:55	371.0	102.4	1007	1.143	0.8653
19:00	376.0	102.4	1006	1.151	0.8667
19:05	381.0	102.4	1006	1.175	0.8712

TABLE 4. DATA FOR EXPERIMENT 20

Clock time	Elapsed time (min)	Pressure (MPa)	Temperature (C)	Can shrinkage (mm)	Relative density
12:45	0.0	0.0	26	0.000	0.6485
12:57	12.0	5.5	27	0.000	0.6485
13:01	16.0	15.2	36	0.000	0.6487
13:12	27.0	20.7	48	0.000	0.6491
13:19	34.0	24.1	53	0.000	0.6492
13:36	51.0	41.4	57	0.032	0.6529
13:59	74.0	80.7	58	0.048	0.6548
14:02	77.0	84.8	57	0.056	0.6557
14:10	85.0	100.0	57	0.056	0.6557
14:47	122.0	97.2	215	-0.016	0.6523
15:02	137.0	97.9	327	-0.048	0.6522
15:24	159.0	98.4	496	-0.063	0.6561
15:57	192.0	99.3	766	-0.127	0.6588
16:09	204.0	100.0	855	-0.127	0.6623
16:17	212.0	100.3	914	-0.095	0.6685
16:20	215.0	100.5	937	0.000	0.6810
16:25	220.0	100.7	973	0.119	0.6974
16:29	224.0	101.0	1000	0.286	0.7205
16:35	230.0	102.7	1050	0.571	0.7635
16:40	235.0	102.7	1054	0.826	0.8032
16:45	240.0	102.7	1050	0.984	0.8293
16:50	245.0	102.7	1053	1.111	0.8518
16:55	250.0	102.7	1054	1.214	0.8707
17:00	255.0	102.7	1054	1.302	0.8872
17:05	260.0	102.7	1053	1.365	0.8995
17:10	265.0	102.7	1053	1.405	0.9073
17:15	270.0	102.7	1055	1.460	0.9187
17:20	275.0	102.7	1054	1.516	0.9302
17:25	280.0	102.7	1054	1.548	0.9368
17:30	285.0	102.7	1053	1.611	0.9504
17:40	295.0	102.7	1054	1.627	0.9539
17:50	305.0	102.7	1052	1.683	0.9660
17:55	310.0	102.7	1052	1.691	0.9678

TABLE 5. DATA FOR EXPERIMENT 21

Clock time	Elapsed time (min)	Pressure (MPa)	Temperature (C)	Can shrinkage (mm)	Relative density
10:09	0.0	0.0	23	0.000	0.6547
10:35	26.0	20.7	45	-0.024	0.6527
10:47	38.0	27.6	51	0.008	0.6565
10:51	42.0	31.0	52	0.008	0.6565
10:57	48.0	36.0	53	0.024	0.6584
11:24	75.0	34.5	168	0.000	0.6591
12:01	112.0	34.5	432	-0.079	0.6586
12:33	144.0	34.6	686	-0.159	0.6587
12:42	153.0	34.8	753	-0.175	0.6594
13:00	171.0	34.5	888	-0.210	0.6607
13:13	184.0	34.5	992	-0.214	0.6645
13:15	186.0	34.5	1000	-0.191	0.6677
13:20	191.0	34.5	1000	-0.159	0.6715
13:23	194.0	34.5	1000	-0.127	0.6753
13:28	199.0	34.5	1000	-0.095	0.6791
13:35	206.0	34.5	1000	-0.063	0.6830
13:40	211.0	34.5	1000	-0.032	0.6870
13:47	218.0	34.5	1000	0.000	0.6909
13:55	226.0	34.5	1000	0.032	0.6950
14:06	237.0	34.5	1000	0.063	0.6990
14:18	249.0	34.5	1000	0.095	0.7031
14:33	264.0	34.5	1000	0.127	0.7072
14:50	281.0	34.5	1000	0.159	0.7114
15:15	306.0	34.5	1000	0.191	0.7156
15:30	321.0	34.5	1000	0.206	0.7177
15:45	336.0	55.8	984	0.222	0.7191
15:48	339.0	71.0	998	0.222	0.7197
15:51	342.0	71.0	984	0.238	0.7212
15:57	348.0	66.2	999	0.262	0.7252
16:18	369.0	73.1	991	0.341	0.7357
16:20	371.0	71.7	999	0.349	0.7372
16:28	379.0	70.3	999	0.381	0.7417
16:37	388.0	70.3	1000	0.413	0.7463
16:48	399.0	70.3	1002	0.445	0.7509
16:56	407.0	70.3	1002	0.476	0.7555
17:09	420.0	70.3	1001	0.508	0.7601
17:22	433.0	70.3	1001	0.540	0.7649
17:36	447.0	70.3	1002	0.571	0.7697

TABLE 6. DATA FOR EXPERIMENT 22a

Clock time	Elapsed time (min)	Pressure (MPa)	Temperature (C)	Can shrinkage (mm)	Relative density
00:30	0.0	0.0	20	0.000	0.6362
00:40	10.0	0.0	20	0.016	0.6380
00:50	20.0	0.0	20	-0.016	0.6345
00:55	25.0	0.0	20	0.016	0.6380
01:30	60.0	0.0	22	0.016	0.6380
01:40	70.0	8.3	29	0.003	0.6368
01:50	80.0	15.4	42	0.013	0.6383
02:00	90.0	22.9	49	0.016	0.6388
02:10	100.0	30.0	51	0.016	0.6389
02:20	110.0	33.1	62	0.022	0.6399
02:30	120.0	33.1	103	0.016	0.6404
02:40	130.0	33.1	174	-0.003	0.6404
02:50	140.0	33.1	253	-0.022	0.6407
03:00	150.0	33.1	332	-0.041	0.6411
03:10	160.0	33.1	411	-0.073	0.6401
03:20	170.0	33.1	481	-0.083	0.6414
03:30	180.0	33.1	549	-0.108	0.6409
03:40	190.0	33.1	619	-0.133	0.6405
03:50	200.0	33.1	697	-0.143	0.6423
04:00	210.0	33.1	765	-0.168	0.6420
04:10	220.0	33.1	827	-0.181	0.6430
04:20	230.0	33.1	909	-0.206	0.6433
04:21	231.0	33.1	918	-0.206	0.6438
04:24	234.0	33.1	939	-0.204	0.6448
04:25	235.0	33.1	946	-0.203	0.6452
04:27	237.0	33.1	961	-0.194	0.6468
04:30	240.0	33.1	980	-0.181	0.6491
04:33	243.0	33.1	999	-0.166	0.6517
04:35	245.0	33.3	1013	-0.156	0.6534
04:36	246.0	33.4	1020	-0.140	0.6556
04:39	249.0	33.8	1046	-0.092	0.6623
04:40	250.0	33.8	1049	-0.076	0.6643
04:42	252.0	33.8	1054	-0.020	0.6713
04:45	255.0	33.8	1054	0.063	0.6816
04:48	258.0	33.8	1053	0.102	0.6864
04:50	260.0	34.0	1048	0.127	0.6893
04:51	261.0	34.1	1046	0.138	0.6906
04:53	263.0	34.1	1050	0.159	0.6936
04:55	265.0	34.1	1050	0.181	0.6964
05:00	270.0	34.1	1049	0.235	0.7033
05:05	275.0	34.1	1050	0.292	0.7110
05:10	280.0	34.1	1053	0.333	0.7167
05:11	281.0	34.1	1053	0.338	0.7174
05:15	285.0	34.1	1052	0.359	0.7201

TABLE 6. Continued

Clock time	Elapsed time (min)	Pressure (MPa)	Temperature (C)	Can shrinkage (mm)	Relative density
05:20	290.0	34.1	1050	0.394	0.7248
05:21	291.0	34.1	1050	0.399	0.7255
05:25	295.0	34.1	1047	0.419	0.7282
05:30	300.0	34.1	1043	0.445	0.7315
05:31	301.0	34.1	1042	0.447	0.7318
05:35	305.0	34.1	1053	0.457	0.7338
05:40	310.0	34.1	1053	0.489	0.7383
05:50	320.0	34.1	1052	0.527	0.7437
06:00	330.0	34.1	1052	0.562	0.7488
06:10	340.0	34.1	1052	0.594	0.7535
06:20	350.0	34.2	1051	0.622	0.7577
06:30	360.0	34.2	1050	0.648	0.7614
06:40	370.0	34.3	1049	0.673	0.7652
06:50	380.0	34.3	1048	0.689	0.7676
07:00	390.0	34.4	1046	0.714	0.7713
07:10	400.0	34.5	1045	0.733	0.7742
07:20	410.0	34.5	1047	0.746	0.7763
07:30	420.0	34.5	1049	0.775	0.7809
07:40	430.0	34.5	1051	0.791	0.7835
07:50	440.0	34.5	1052	0.806	0.7861
08:00	450.0	34.5	1051	0.816	0.7875
08:10	460.0	34.5	1051	0.835	0.7906
08:20	470.0	34.5	1051	0.841	0.7916
08:30	480.0	34.5	1052	0.854	0.7937
08:40	490.0	34.5	1052	0.870	0.7963
08:50	500.0	34.5	1051	0.873	0.7967
09:00	510.0	34.5	1050	0.886	0.7987
09:10	520.0	34.5	1049	0.892	0.7997
09:20	530.0	34.5	1048	0.905	0.8017
09:30	540.0	34.5	1047	0.908	0.8022
09:40	550.0	34.5	1052	0.918	0.8041
09:50	560.0	37.2	1047	0.908	0.8022
09:52	562.0	40.0	1043	0.908	0.8019
09:56	566.0	45.5	1050	0.908	0.8024
09:58	568.0	48.3	1045	0.908	0.8021
10:00	570.0	51.7	1047	0.908	0.8022
10:02	572.0	55.2	1049	0.911	0.8027
10:05	575.0	60.3	1048	0.914	0.8033
10:06	576.0	62.1	1048	0.918	0.8039
10:09	579.0	68.9	1047	0.930	0.8057
10:10	580.0	72.1	1047	0.933	0.8064
10:13	583.0	81.4	1047	0.949	0.8089
10:14	584.0	77.2	1050	0.954	0.8100
10:15	585.0	77.8	1049	0.959	0.8107
10:20	590.0	80.9	1045	0.994	0.8164

TABLE 6. Continued

Clock time	Elapsed time (min)	Pressure (MPa)	Temperature (C)	Can shrinkage (mm)	Relative density
10:23	593.0	82.7	1042	0.999	0.8171
10:25	595.0	87.3	1045	1.003	0.8180
10:26	596.0	89.6	1047	1.010	0.8192
10:29	599.0	96.5	1047	1.029	0.8225
10:30	600.0	99.3	1049	1.035	0.8237
10:31	601.0	102.0	1050	1.042	0.8249
10:35	605.0	100.2	1051	1.070	0.8299
10:37	607.0	99.3	1051	1.083	0.8321
10:40	610.0	98.6	1051	1.102	0.8354
10:43	613.0	97.9	1050	1.119	0.8384
10:45	615.0	97.9	1050	1.130	0.8404
10:50	620.0	97.9	1051	1.149	0.8439
10:53	623.0	97.9	1051	1.159	0.8456
10:55	625.0	97.9	1051	1.165	0.8468
11:00	630.0	97.9	1051	1.197	0.8525
11:10	640.0	99.8	1051	1.222	0.8572
11:20	650.0	101.0	1050	1.251	0.8624
11:30	660.0	100.7	1051	1.286	0.8691
11:40	670.0	100.7	1052	1.311	0.8740
11:50	680.0	100.7	1052	1.327	0.8770
12:00	690.0	100.7	1051	1.349	0.8812
12:10	700.0	100.7	1052	1.362	0.8838
12:20	710.0	100.7	1052	1.384	0.8881
12:30	720.0	100.7	1051	1.407	0.8924
12:40	730.0	100.7	1050	1.416	0.8942
12:50	740.0	100.7	1051	1.435	0.8981
13:00	750.0	100.7	1051	1.445	0.9000
13:10	760.0	100.7	1049	1.454	0.9018
13:20	770.0	100.7	1052	1.464	0.9039
13:30	780.0	100.7	1051	1.486	0.9084
13:40	790.0	100.7	1051	1.505	0.9123
13:50	800.0	100.7	1061	1.511	0.9144
14:00	810.0	100.7	1074	1.514	0.9161
14:10	820.0	100.7	1094	1.521	0.9190
14:20	830.0	100.7	1104	1.546	0.9252
14:30	840.0	100.7	1134	1.562	0.9311
14:40	850.0	100.7	1153	1.616	0.9444
14:50	860.0	100.7	1150	1.654	0.9526
15:00	870.0	100.7	1151	1.676	0.9576
15:10	880.0	100.6	1153	1.699	0.9628
15:20	890.0	100.3	1150	1.708	0.9647
15:30	900.0	100.3	1151	1.714	0.9663
15:40	910.0	100.3	1152	1.721	0.9678
15:44	914.0	100.3	1152	1.721	0.9678

TABLE 7. DATA FOR EXPERIMENT 22c

Clock time	Elapsed time (min)	Pressure (MPa)	Temperature (C)	Can shrinkage (mm)	Relative density
01:18	0.0	34.5	40	0.000	0.6272
01:27	9.0	34.5	68	0.003	0.6282
01:36	18.0	34.5	139	-0.013	0.6285
01:48	30.0	34.5	236	-0.036	0.6288
01:57	39.0	34.5	310	-0.055	0.6290
01:58	40.0	34.5	317	-0.057	0.6289
02:07	49.0	34.5	387	-0.079	0.6288
02:16	58.0	34.5	451	-0.095	0.6290
02:25	67.0	34.5	520	-0.119	0.6287
02:34	76.0	34.8	589	-0.135	0.6293
02:43	85.0	35.2	658	-0.156	0.6293
02:52	94.0	35.2	727	-0.178	0.6294
03:01	103.0	35.2	788	-0.197	0.6295
03:09	111.0	35.2	846	-0.213	0.6299
03:19	121.0	35.2	917	-0.218	0.6319
03:22	124.0	35.2	938	-0.217	0.6328
03:25	127.0	35.2	966	-0.212	0.6343
03:28	130.0	35.2	988	-0.191	0.6374
03:37	139.0	35.2	1050	-0.022	0.6583
03:45	147.0	35.2	1053	0.168	0.6801
03:54	156.0	35.2	1053	0.296	0.6955
04:03	165.0	35.2	1051	0.382	0.7061
04:12	174.0	35.2	1050	0.453	0.7151
04:21	183.0	35.5	1050	0.507	0.7220
04:30	192.0	35.9	1051	0.555	0.7283
04:39	201.0	35.9	1050	0.591	0.7330
04:48	210.0	35.9	1050	0.618	0.7368
04:57	219.0	35.9	1053	0.659	0.7424
05:06	228.0	35.9	1050	0.687	0.7461
05:15	237.0	35.9	1051	0.704	0.7484
05:24	246.0	35.9	1050	0.735	0.7528
05:33	255.0	35.9	1050	0.758	0.7560
05:42	264.0	35.9	1051	0.782	0.7594
05:51	273.0	35.9	1051	0.800	0.7620
06:00	282.0	35.9	1052	0.810	0.7635
06:09	291.0	35.9	1051	0.826	0.7656
06:18	300.0	35.9	1050	0.845	0.7683
06:27	309.0	35.9	1050	0.861	0.7707
06:36	318.0	35.9	1050	0.875	0.7727
06:45	327.0	35.9	1050	0.889	0.7748
06:54	336.0	35.9	1050	0.903	0.7768
07:03	345.0	35.9	1050	0.914	0.7785
07:12	354.0	35.9	1050	0.927	0.7804
07:18	360.0	35.9	1049	0.933	0.7813

TABLE 7. Continued

Clock time	Elapsed time (min)	Pressure (MPa)	Temperature (C)	Can shrinkage (mm)	Relative density
07:27	369.0	48.3	1050	---	---
07:36	378.0	62.1	1046	---	---
07:45	387.0	73.1	1045	---	---
07:54	396.0	89.6	1046	---	---
08:01	403.0	104.1	1050	1.102	0.8071
08:10	412.0	102.0	1049	1.172	0.8182
08:19	421.0	101.4	1050	1.226	0.8269
08:28	430.0	100.7	1050	1.274	0.8348
08:37	439.0	99.3	1050	1.312	0.8412
08:46	448.0	99.3	1051	1.347	0.8473
08:55	457.0	98.9	1052	1.373	0.8517
09:04	466.0	98.6	1053	1.398	0.8562
09:13	475.0	98.3	1052	1.433	0.8621
09:22	484.0	102.0	1051	1.457	0.8663
09:31	493.0	101.4	1050	1.485	0.8712
09:40	502.0	100.7	1050	1.506	0.8751
09:48	510.0	100.7	1051	1.525	0.8786
09:57	519.0	100.7	1123	1.535	0.8855
10:00	522.0	100.7	1147	1.556	0.8910
10:00	522.5	100.7	1150	1.561	0.8921
10:10	532.0	100.7	1150	1.660	0.9110
10:19	541.0	100.0	1150	1.722	0.9232
10:28	550.0	99.6	1150	1.750	0.9287
10:37	559.0	99.3	1150	1.765	0.9318
10:46	568.0	99.3	1150	1.773	0.9333
10:55	577.0	99.3	1153	1.778	0.9346
11:04	586.0	103.4	1149	1.784	0.9356
11:10	592.0	103.4	1150	1.789	0.9367
11:13	595.0	102.0	1150	1.789	0.9367
11:22	604.0	101.4	1150	1.789	0.9367
11:31	613.0	101.4	1152	1.789	0.9368

by the methods described below.

Before experiment 22c, a change was made in the gas supply lines for the autoclave. This design change apparently resulted in stronger gas currents within the autoclave during pressurization. The gas currents disturbed the probe so that reliable measurements of the can shrinkage could not be obtained during pressurization from 35.8 to 104.1 MPa. As a result, listings of can shrinkage and relative density are missing for a small portion of the Table 7.

Figures 2 through 7 reproduce in graphical form the temperatures, pressures, and densities in the tables. As expected, major changes in temperature or pressure cause clearly visible changes in the densification rate.

Conversion of can shrinkage to current relative density also requires the measurements shown in Table 8. Figure 8 shows the positions at which the various dimensions are measured. The initial relative density is obtained from the initial weight, length, and diameter of the sample. Except for can diameter and length, the initial dimensions must be measured before assembly of the can. Most of the final dimensions require cutting of the can and sample. While six measurements are necessary to describe the initial geometry, only four are necessary after HIP since the gap between sample and can is gone.

Reduction of data starts with taking data for temperature, pressure, and can shrinkage from strip-chart records and keying it into a computer. Data points are chosen so that the discrete points will provide a good description of the actual experiment. Since the time interval between the data points is generally small, linear interpolation is used between readings. Physical dimensions and initial density, as shown in Table 8,are inserted at the beginning of the data file.

The data is converted to densities by a Fortran program that is listed in the appendix. Before discussing the algorithm used in the program, however, it is appropriate to describe the assumptions made and the estimated error due to the assumptions.

The integrated thermal expansions of alumina and stainless steel are given by

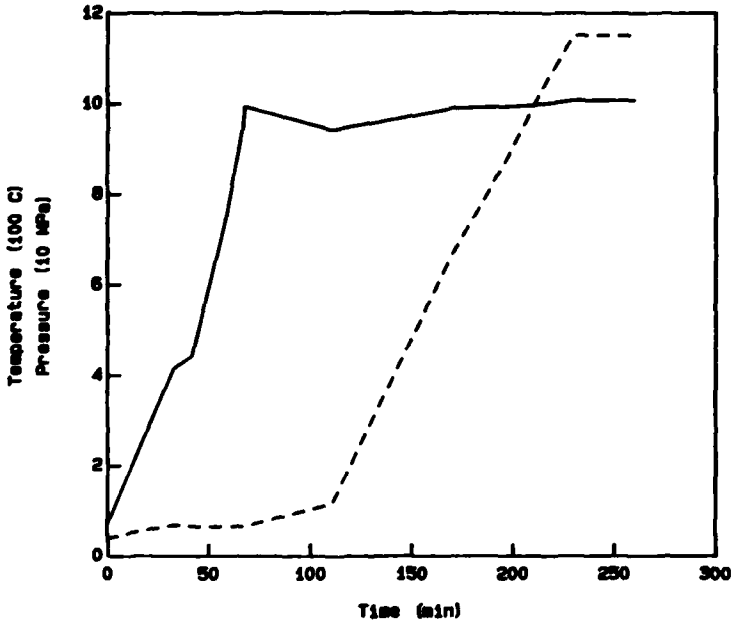

2a.

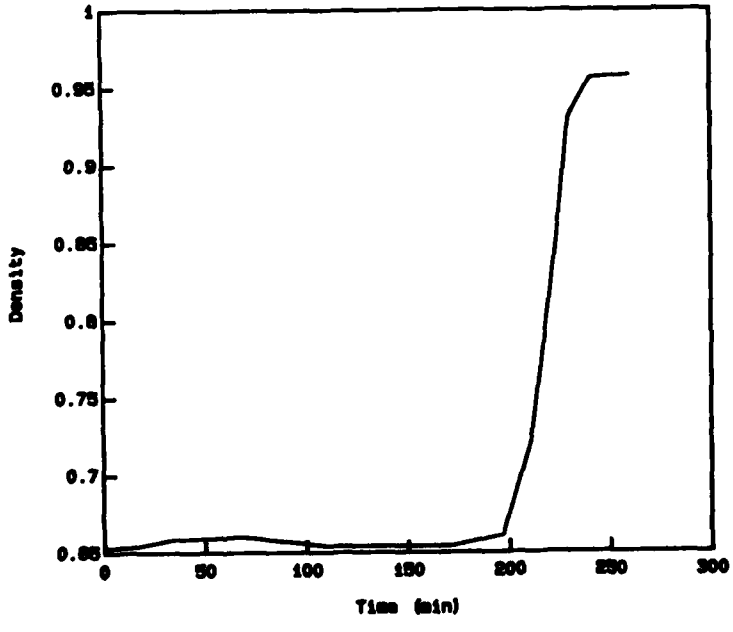

2b.

Figure 2. Data for experiment 14. a) Pressure (solid line) and temperature (dotted line). b) Density as calculated from temperature and can shrinkage.

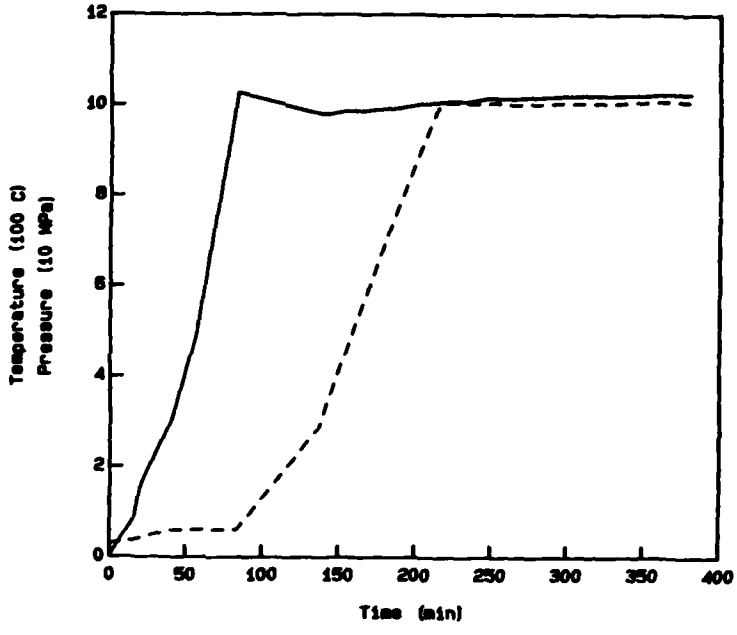

3a.

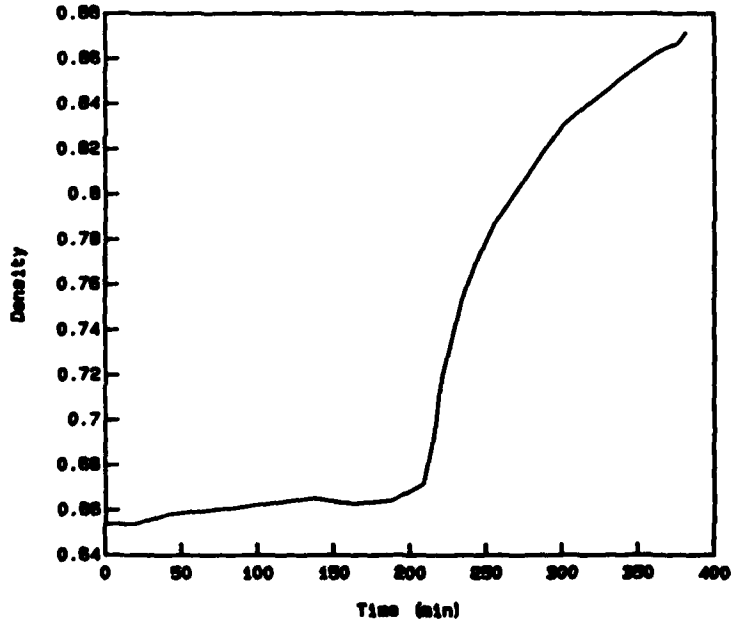

3b.

Figure 3. Data for experiment 19. a) Pressure (solid line) and temperature (dotted line). b) Density as calculated from temperature and can shrinkage.

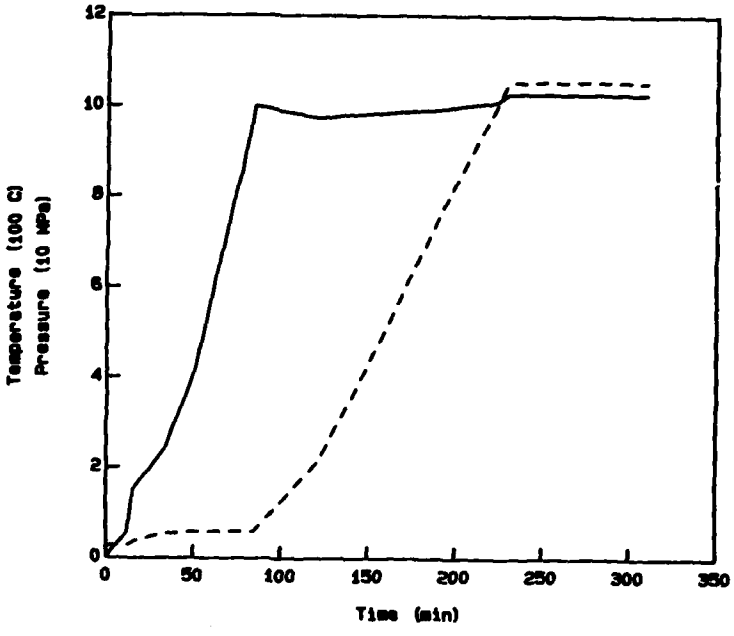

4a.

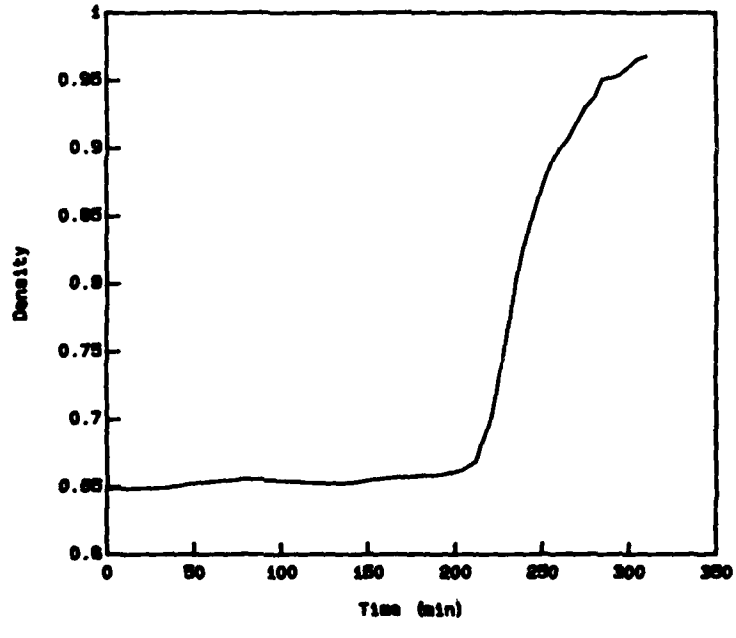

4b.

Figure 4. Data for experiment 20. a) Pressure (solid line) and temperature (dotted line). b) Density as calculated from temperature and can shrinkage.

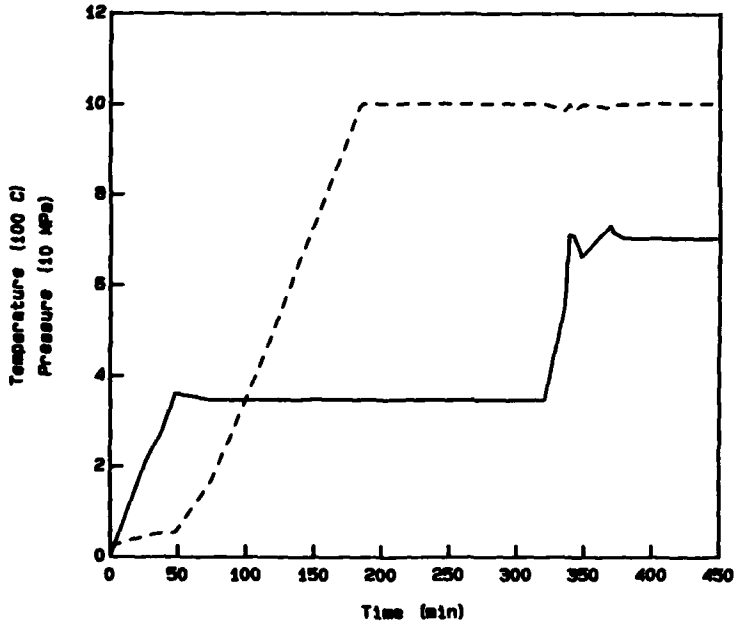

5a.

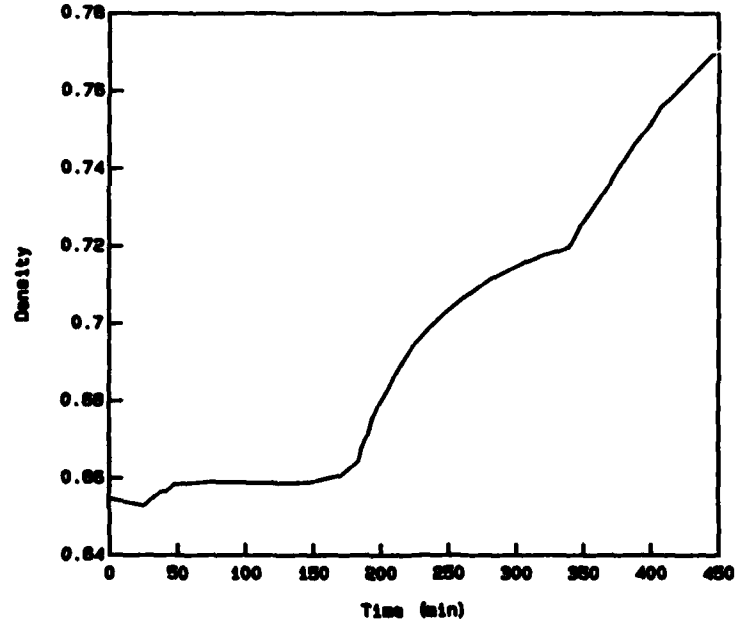

5b.

Figure 5. Data for experiment 21. a) Pressure (solid line) and temperature (dotted line). b) Density as calculated from temperature and can shrinkage. Density curve clearly shows effect of changing pressure from 34 to 70 MPa at 330 min.

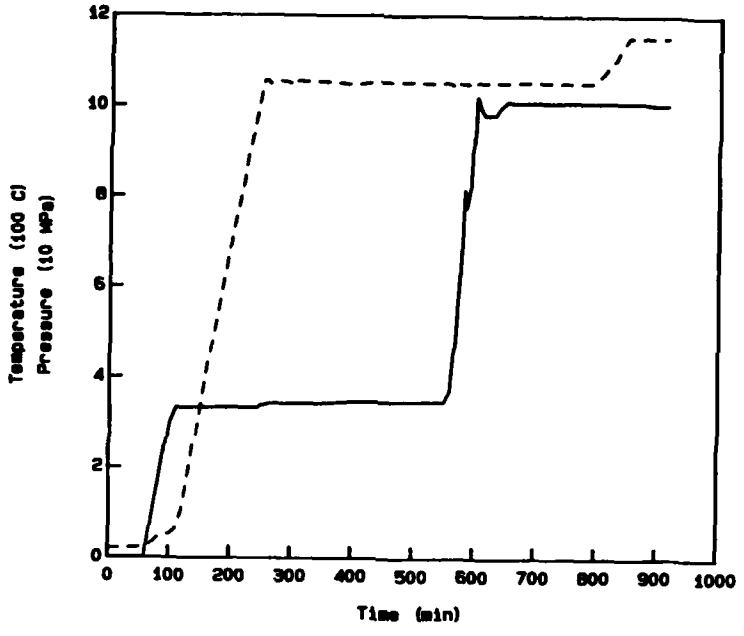

6a.

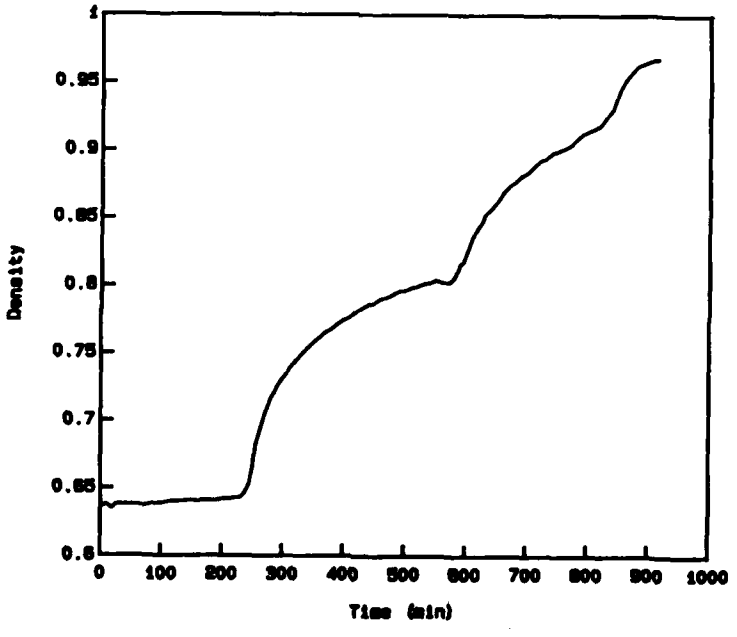

6b.

Figure 6. Data for experiment 22a. a) Pressure (solid line) and temperature (dotted line). b) Density as calculated from temperature and can shrinkage. Density curve clearly shows effect of changing pressure from 34 to 100 MPa at 580 min and changing temperature from 1050 to 1150°C at 830 min.

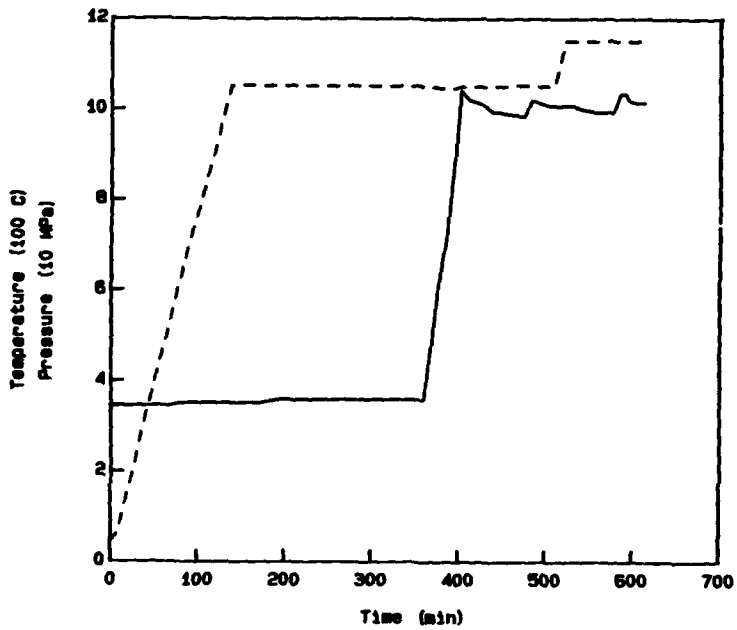

7a

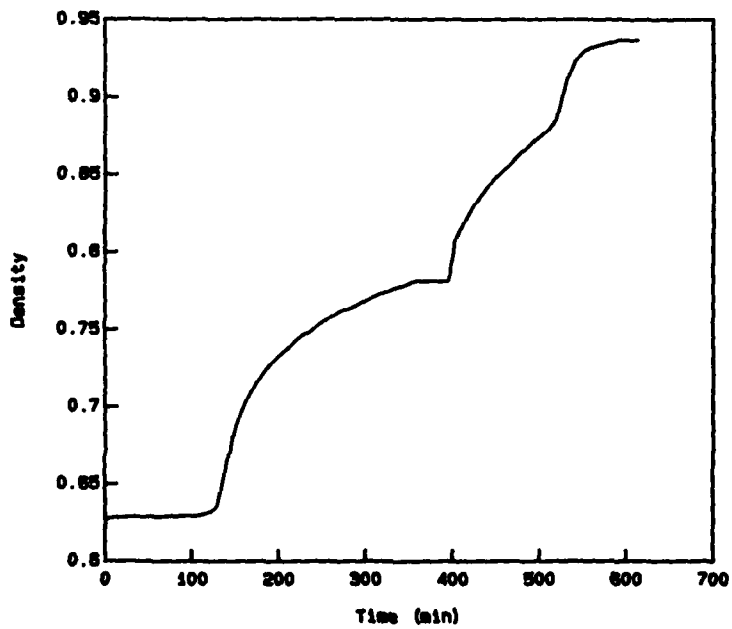

7b.

Figure 7. Data for experiment 22c. a) Pressure (solid line) and temperature (dotted line). b) Density as calculated from temperature and can shrinkage. Density curve clearly shows effect of changing pressure from 36 to 100 MPa at 390 min and changing temperature from 1050 to 1150°C at 520 min. Density is not totally reliable between 361 and 396 minutes.

TABLE 8. PHYSICAL MEASUREMENTS OF HIP SAMPLES AND CANS

Measurement, mm (except density)	Run number					
	14	19	20	21	22a	22c
Initial sample length	39.67	39.68	39.70	39.66	39.67	39.67
Initial can length	51.32	52.24	49.90	50.91	50.82	50.95
Final can length	46.82	47.90	45.28	49.04	46.35	46.50
Initial end plug length	11.10	11.13	9.45	10.97	11.10	11.10
Final end plug length	11.69	11.60	10.08	11.16	11.79	11.64
Initial sample diameter	22.00	22.00	22.00	22.00	22.01	22.01
Initial can diameter	25.39	25.37	25.38	25.36	25.37	25.37
Final sample diameter	23.28	23.85	23.33	24.53	23.11	22.88
Initial can wall thickness	1.57	1.57	1.57	1.57	1.66	1.66
Final can wall thickness	2.12	1.98	2.08	1.83	2.18	2.11
Initial relative density	.6562	.6556	.6556	.6549	.6370	.6374

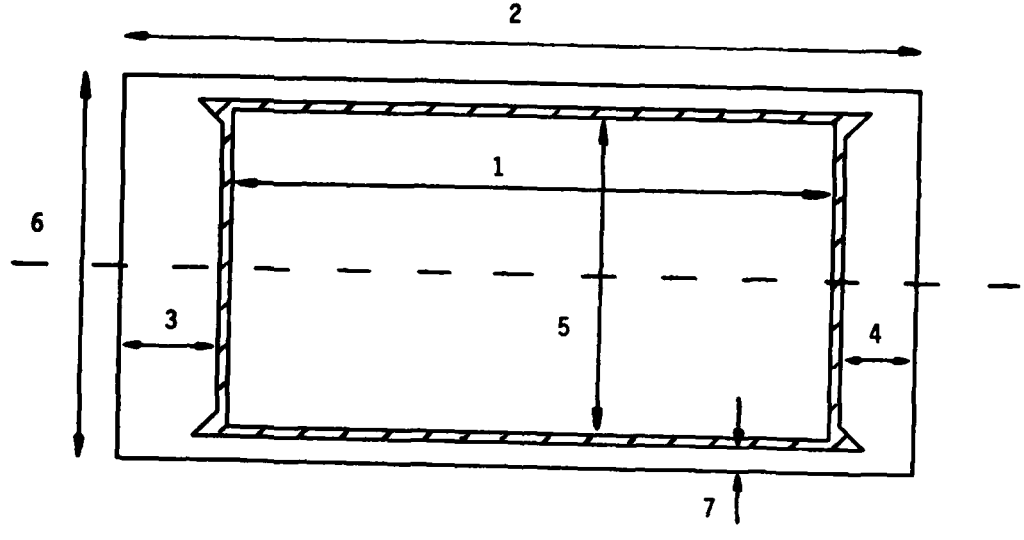

FIGURE 8. CROSS SECTION OF HIP CAN AND SAMPLE SHOWING MEASUREMENTS.
1 = sample length, 2 = can length, 3 + 4 = end plug length,
5 = sample diameter, 6 = can diameter, 7 = can wall thickness.
Gap between can and sample (shaded area) is exaggerated.
Dashed line is axis of can.

$$\varepsilon_{Al_2O_3} = 7.2978E\text{-}6\ (T-293) + 7.8486E\text{-}10\ (T-293)\ (T-800) \qquad (1a)$$

$$\varepsilon_{304ss} = 1.7751E\text{-}5\ (T-293) + 5.0423E\text{-}9\ (T-293)\ (T-800). \qquad (1b)$$

In these equations, we have used E to denote multiplication by the specified power of 10, following the standard computational convention. Note that these are are the integrals of the ordinary coefficients of linear thermal expansion. These equations were obtained by fitting a quadratic to data compiled by Touloukian[1].

Thermal expansion will also affect the geometry of the probe mechanism itself. Quite a few thermal effects might be anticipated. The probe rods will change in length and diameter both above and below the pivots. The pivots themselves will expand and move. The sample will be displaced as its supporting structure expands. Where the temperature gradient has a component normal to the axis of the probe rods, the rods will deflect. It is not feasible to perform an accurate calculation of all the thermal expansion effects, so it would appear that the best approach to this problem would be to calibrate the probe carefully against a dummy sample of some non-densifiable material with a well-known coefficient of thermal expansion. Even if such a calibration were performed, there might still be unconsidered effects from thermal transients. Our calculations to date have used the simple approach of assuming that all these thermal expansions have a negligible net effect on the measured can diameter. This assumption is supported by the apparently small systematic errors in the final calculated densities when compared to immersion densities, as discussed below.

It is assumed that the material of the can is always at full density and that the mass of the sidewall of the can is constant. The stainless steel can is rather soft at HIP temperatures, so incompatibility of thermal expansion between sample and can is handled as follows: For any given density, the alumina is assumed to expand isotropically upon heating. The can expansion cannot be isotropic, however, since it expands faster than the alumina, and the applied gas pressure will keep the can in contact with the sample. Our assumption that the mass of the sidewall is constant is equivalent to assuming that the can does not

slip axially along the sample, and that the extra thermal expansion of the can is taken up as a plastic thickening of the can wall. Using the final dimensions from can 14, the combined thermal expansion of the sample and can upon heating from 20°C to 1150°C will be 0.378 mm. This corresponds to a change in the relative density of 0.08, which is typical. Thermal expansion is undoubtedly the most important single correction in the conversion of probe readings to densities.

For a fixed density (expressed as fraction of theoretical density) it is assumed that the thermal expansion of alumina is isotropic. However, experimental measurements show that the length-to-diameter ratio of the sample changes as the density changes. Diameter is recorded continuously, but length is measured only at the beginning and end of the run. Therefore, it is necessary to assume some relationship between the length and diameter during the run. It is currently assumed that

$$\frac{L(\rho,20)}{L(\rho_i,20)} = \left(\frac{d(\rho,20)}{d(\rho_i,20)}\right)^{\alpha} \qquad (2)$$

where $d(\rho, 20)$ and $L(\rho, 20)$ denote the sample diameter and length, respectively, at the fractional density in question and 20°C. The subscript i denotes an initial value. The exponent α is set by the initial and final measured lengths and diameters of the sample. A typical value of α is 0.85. This is not far from the ideal value $\alpha = 1.0$, which describes a constant length-to-diameter ratio.

The assumption of Equation 2 is essentially arbitrary, and other relations such as

$$\frac{L(\rho,20) - L(\rho_i,20)}{L(\rho_i,20) - L(\rho_f, 20)} = \frac{d(\rho,20) - d(\rho_i,20)}{d(\rho_f,20) - d(\rho_i,20)} \qquad (3)$$

might be suggested, where the subscript f denotes a final value. Using the measurements from experiment 14, one finds that, for any diameter between the initial and final diameter, the maximum discrepancy in calculated sample length as given by Equations 2 and 3 is about 0.013 mm. This corresponds to an error in density of less than 0.04%, which is

negligible in our experiments.

It is assumed that the initial gap between the sample and the can shown in Figure 8 vanishes during HIP. Thus the final sample diameter is the final outside diameter of the can minus twice the final can wall thickness, and the final sample length is the final can length minus the length of the end plugs. This assumption is supported by examination of the samples; no gaps were found after HIP. A thin reaction layer consisting of oxides of aluminum, iron, chromium, and nickel was detected between the alumina sample and the stainless steel can. Measurements of the reaction layer indicate that an error of less than 0.05% results from ignoring the layer.

Using these assumptions, the program proceeds in the following way. For a given time, the pressure, temperature, and shrinkage are measured, and the actual outside diameter of the can is calculated by subtracting the shrinkage from the original size. Then the problem is attacked from the other direction: A fractional density is assumed, and the diameter and length of the sample at 20°C are calculated by means of Equation 2. Using Equation 1a, the dimensions of the sample at temperature are calculated. The volume of the can sidewall at 20°C is corrected for temperature by converting the linear expansion of Equation 1b to a volume expansion, and the necessary wall thickness to produce that volume is calculated. For the assumed density, the outside diameter of the can will be the sample diameter plus twice the wall thickness. The program repeats this process with different values of density until it finds an outside diameter which is equal to the actual outside diameter of the can. As output, the program produces a table in which each line contains time, temperature, pressure, can shrinkage, and relative density. Plots like those of Figures 2 to 7 are readily made by passing selected columns to a plotting package.

One difficulty with this approach is that different methods for measuring the volume of the can sidewall give different volumes. The volume of the sidewall at 20°C is given by

$$V = \pi w(D-w)L \qquad (4)$$

where w is the sidewall thickness, D is the outside diameter of the can, and L is the length of the sidewall, all measured at 20°C. It is reasonable to assume that the volume of the sidewall as measured at 20°C is constant, that is, that the mass of the sidewall is constant. The sidewall volume may be logically defined in at least three ways: 1. w may be assumed to be the initial can wall thickness, D may be assumed to be the initial outside diameter of the can, and L may be assumed to be the initial can length minus the initial length of the end plugs. 2. w may be assumed to be the initial can wall thickness, D may be assumed to be the initial outside diameter of the can, and L may be assumed to be the initial sample length. 3. w may be assumed to be the final can wall thickness, D may be assumed to be the final outside diameter of the can, and L may be assumed to be the final sample length. Note that the length used in method 1 is longer than the length used in method 2, the difference being the length of the air gaps at the end of the sample. Method 3 differs from the others by using final measurements instead of initial measurements. Table 9 shows the sidewall volumes as determined by each of the three methods just described. As expected, the volumes determined by method 2 are consistently smaller than those determined by method 1, since method 2 assumes a slightly longer sidewall. However, there is no apparent relationship between the volumes obtained by method 3 and those obtained by methods 1 or 2. The discrepancies between the various volumes are unexpectedly large. The choice of the sidewall volume affects the density that is calculated from the can shrinkage. For the data obtained to date, the three methods for measuring sidewall volume can yield calculated relative densities that differ by as much as 4.6%. The choice of the correct can sidewall volume is an important unsolved problem. It must be studied in more detail if the probe is to provide more accurate values of density.

We have used method 3 to obtain the sidewall volume, since this method requires no assumptions concerning the nature of the collapse of the can onto the sample. As shown in Table 10, there has generally been good correlation between the final density as calculated from the probe data and as measured by immersion. If experiment 22c is

TABLE 9. CAN SIDEWALL VOLUMES AS DETERMINED BY VARIOUS METHODS

Run	Sidewall volume, cm^3		
	Method 1	Method 2	Method 3
14	4.73920	4.67457	4.96023
19	4.83961	4.67128	4.94096
20	4.76382	4.67497	4.88847
21	4.69937	4.66738	4.95432
22a	4.92189	4.91686	4.95809
22c	4.93921	4.91686	4.80638

TABLE 10. COMPARISON OF FINAL DENSITIES AS CALCULATED FROM PROBE DATA AND AS MEASURED BY IMMERSION

Experiment Number	Final Density		Difference
	Calc.	Meas.	
14	.9576	.960	-.002
19	.8712	.876	-.005
20	.9678	.952	.016
21	.7697	.758	.012
22a	.9678	.984	-.016
22c	.9368	1.000	-.063

excluded, the root-mean-square difference between the calculated and immersion densities is 1.3%. There is no evident systematic error, so our assumptions concerning thermal expansion appear to be justified.

The unusually large discrepancy for experiment 22c has not been explained completely. It is known that there were certain irregularities in the experimental procedure. For example, a reliable calibration of the probe to the initial diameter of the can was not obtained due to equipment difficulties during pressurization. We have included the data for this experiment, however, since the changes in density should be reliable even though the values are systematically in error.

THEORY OF DENSIFICATION

In this section a theory of densification by grain-boundary diffusion with interface reaction control is developed. We discuss the role of grain-boundary dislocations in limiting the rate of grain-boundary diffusion and review the geometry of interparticle necks and the effect of neck geometry on the effective contact stress. We present the results of comparing this theory of densification with experimental data and argue that interface-reaction controlled grain-boundary diffusion is the mechanism that best explains the data. Limitations of the theory and potential for future development are discussed. A glossary, Table 11, is provided as a quick reference for the variables used in this section.

Densification by grain-boundary diffusion has been thoroughly treated in the literature. The effect of grain-boundary dislocations in limiting grain-boundary diffusion has also been discussed, though usually with regard to creep rather than densification. The effect of grain-boundary dislocations may be pictured roughly as follows. Consider two particles in a sample that is densifying by grain-boundary diffusion. Densification occurs when matter flows from the contact area between the two particles to the surface of the neck, and the two particles approach each other. Under certain conditions, the rate determining step is not diffusion but the detaching of atoms from the grains. The energetically favored place for an atom to detach from a grain is at a grain-boundary dislocation. If the two grains were separated, the grain-boundary dislocations would be ledges on the new surface. As densification proceeds, the dislocation climbs along the grain boundary. As shown in Figure 9, solute atoms tend to segregate to the dislocation, and climb may be limited by solute drag if the diffusivity of the solute is low.

The terminology "interface-reaction controlled" is actually a misnomer. While it is true that the amount of mass transport by grain-boundary diffusion is limited by the difficulty of moving grain-boundary dislocations, the actual rate-limiting process is the diffusion of

TABLE 11. GLOSSARY OF TERMS

a	average neck area
b_b	Burgers vector
b_n	component of Burgers vector normal to grain boundary
c	derivative of coordination number with respect to R'/R, $c = 15.5$
C_o	bulk solute concentration
C_1	constant, $C_1 = 0.5$
D	relative density
D_o	initial relative density
D_r	relative density of random dense packing, $D_o = 0.64$
D_s^o	diffusivity of solute at infinite temperature
D_s	diffusivity of solute
E_s	activation energy for diffusion of solute
F	force per unit length on dislocation
G	shear modulus
k	Boltzmann's constant
M	dislocation mobility
p	external pressure
p^*	effective contact stress
P_s	contact pressure due to surface tension
P_{th}	threshold contact pressure

TABLE 11. Continued

R	particle radius
R'	current particle radius in Arzt's growing-sphere description
$\mathcal{R}$	gas constant
T	temperature
t	time
v_{dis}	dislocation velocity
w	neck axial radius of curvature
y	particle center-to-center distance
Z	coordination number
Z_o	coordination number at D_o, $Z_o = 7.3$
α_o	constant, $\alpha_o = 0.2$
β	ratio of solute concentration near dislocation to solute concentration in bulk
γ	surface tension
ρ	dislocation density
Ω	effective atomic volume of solute

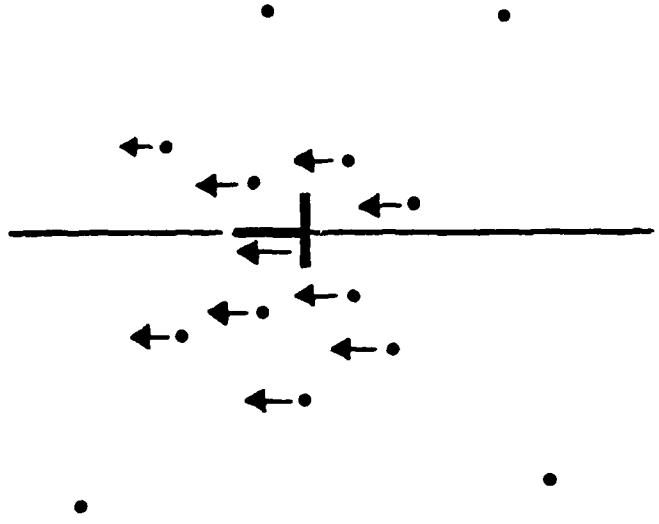

Figure 9. Grain boundary dislocation with an atmosphere of solute atoms. As the dislocation climbs along the grain boundary, solute atoms exert a drag force.

solute in the lattice. The motion of a small number of solute atoms in the lattice can result in a large number of atoms being freed from a grain-boundary dislocation. Once they are free from the dislocation, the atoms quickly diffuse away.

Following Arzt, Ashby, and Verrall[2], the rate at which an individual grain boundary dislocation climbs is

$$v_{dis} = MF = Mp^* b_n. \tag{5}$$

Here F is the force per unit length on the dislocation and M is the dislocation mobility. From elementary dislocation theory, it follows that the force on the dislocation is the product of the effective contact pressure p* and the component of the Burgers vector normal to the grain boundary b_n.

Applying the results of Cottrell and Jaswon[3] and Cottrell[4], Arzt, Ashby, and Verrall obtained the following expression for grain-boundary dislocation mobility limited by solute drag:

$$M = \frac{D_s \Omega}{\beta k T b_b^2 C_o} \tag{6}$$

In this equation, C_o is the concentration of solute in the lattice, and the concentration in the solute atmosphere of the dislocation is increased by a factor β to βC_o. D_s is the diffusivity of the solute in the lattice, Ω is the effective atomic volume of the solute, kT has its usual meaning, and b_b is the Burgers vector of the grain-boundary dislocation.

To complete the description of a grain-boundary with dislocations we need only an expression for the density of dislocations. This problem has been studied by Burton[5] and by Arzt, Ashby, and Verrall[2]. Although different approaches were used, their results are in substantial agreement. Arzt's result is

$$\rho = \frac{C_1 p^*}{G b_b} \tag{7}$$

where C_1 is a constant (about 0.5), G is the shear modulus, and b_b is

the length of the Burgers vector.

Before proceeding further, it is necessary to consider again the geometry of densification at the scale of complete grains. The most important geometrical quantities are illustrated in Figure 10: R is the particle radius, y is the particle center-to-center distance, x is the neck radius, and w is the neck axial radius of curvature. If it is assumed that the sample starts as a packing of tangential spherical particles and that the particles approach each other as densification proceeds, it is clear from geometry that

$$D = D_o(2R/y)^3 \tag{8}$$

where D_o is the initial density and D is the current density. By differentiating Equation 8, one obtains

$$\frac{dD}{dt} = -\frac{3D}{2R}\left(\frac{D}{D_o}\right)^{1/3}\frac{dy}{dt} \tag{9}$$

where dy/dt is the rate of change of the particle center-to-center distance. This result is at variance with Equation 2 of Arzt, Ashby, and Easterling[6]. Their result can be derived from the assumption that

$$D = D_o(y/2R)^3. \tag{10}$$

This equation is clearly incorrect; it predicts a decrease in density as the particles move toward each other. Our Equations 8 and 9 correct this error.

A change in y results from the motion of grain-boundary dislocations. The passage of one dislocation across the entire neck reduces the center-to-center distance y by b_n where b_n is the component of the Burgers vector normal to the grain boundary. In the case where several dislocations are moving together, the number of dislocations that will pass a given point on the grain boundary in unit time is $v_{dis}\rho$. Thus the rate of approach of two particles is

$$dy/dt = -v_{dis}\rho b_n \tag{11}$$

It has been indicated in Equation 5 that the driving force for

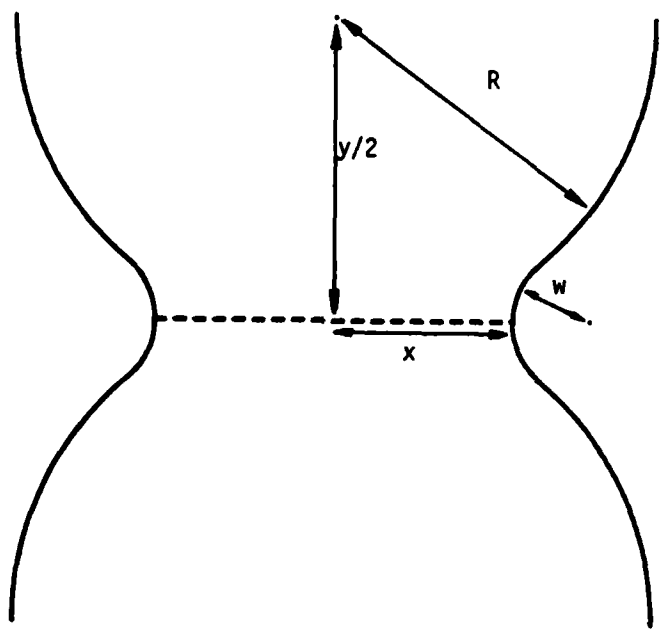

Figure 10. Geometry of two spherical particles and a toroidal neck.

densification is the effective contact pressure p* between the two particles. Following Arzt, Ashby, and Easterling[6], we write this pressure as

$$p^* = \frac{4\pi R^2 p}{aZD} + p_s - p_{th} \tag{12}$$

where p is the external applied pressure, a is the average neck area, Z is the coordination number, p_s is the contact pressure due to surface tension, and p_{th} is a threshold pressure below which the grain-boundary dislocations cannot move. Since our material was thoroughly outgassed before canning and the cans welded in vacuum, the effect of gas trapped in the pores is neglected.

Coordination number and contact area have been treated in some detail by Arzt[7]. For mathematical convenience, Arzt describes densification not as a packing of spheres that approach each other but as a packing of stationary spheres that grow fictitiously. If the spheres grow from a radius R to a radius R', the increase in the volume of the spheres will cause the density to increase from its initial value D_o to a new value D, where

$$D/D_o = (R'/R)^3. \tag{13}$$

As the spheres begin to grow, it is evident that they must deform to keep from overlapping with their neighbors. Arzt has treated this problem in the following way. At the beginning of densification, space is partitioned into Voronoi cells, as shown in Figure 11. The Voronoi cell of a given particle consists of all points that are closer to the center of that particle than to the center of any other particle. Since it has been assumed that the particles are stationary, it is also reasonable to assume that the Voronoi cells do not change during densification. Let us consider a single sphere as shown in Figure 12. The sphere is tangent to the boundary of its Voronoi cell at any point where it coordinates another sphere. If we now imagine the sphere growing without deforming, parts of the sphere will fall outside the Voronoi cell, as shown in Figure 12b. At the same time, we must also imagine

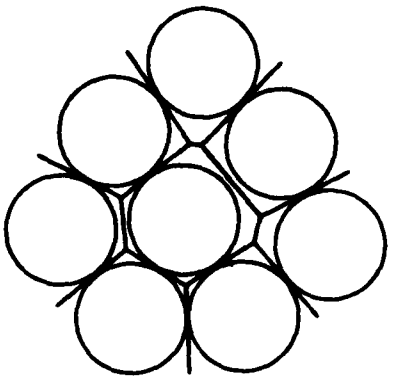

Figure 11. A two-dimensional schematic of a random packing of spheres and their Voronoi cells, after Arzt.

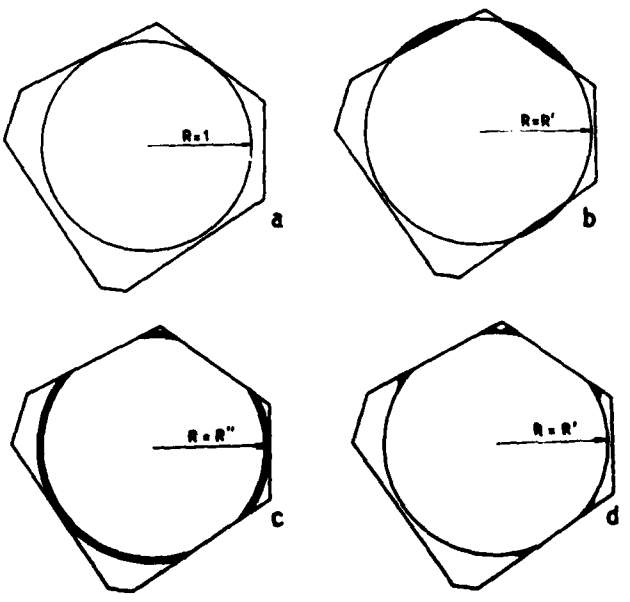

Figure 12. A typical particle in a random dense packing and its Voronoi cell, after Arzt. a) No densification has occurred. b) The particle grows fictitiously without deformation to radius R', overlapping neighboring particles. To prevent overlap, deformation of the particle occurs, with material being distributed either c) uniformly over the free surface or d) in necks around the contact region.

the coordinating spheres growing. These spheres will also grow beyond their fixed Voronoi cells, and the spheres will overlap. Real particles do not overlap during densification, so it is clear that some deformation of the spheres must take place. Arzt has assumed that when a sphere grows to the point that part of its volume would be outside the Voronoi cell boundary, the sphere deforms so that the material which would fall outside the cell is redistributed inside the cell. Under this assumption, one may think of the sphere as growing inside a rigid Voronoi cell. The assumption is actually quite reasonable. Wherever sphere A would grow past its cell boundary into the cell of sphere B, sphere B would also grow past its cell boundary into the cell of sphere A. Since the two spheres are identical, they would force each other to remain within their respective cells.

Arzt considered two ways in which the material might be redistributed when the spheres deform. Figure 12c shows the material uniformly spread over the free surface of the particle. This would be realistic for cold compaction of a ductile powder. Figure 12d shows the material deposited only in the necks. We have assumed that all displaced material remains in the necks, since it is expected that surface tension would result in a well-rounded neck like that shown in Figure 12d rather than a sharp neck like that in Figure 12c.

As the spheres continue to grow, they begin to coordinate additional spheres that they did not coordinate in the original packing. Using radial distribution functions for a random dense packing developed by Scott[8] and Mason[9], Arzt developed the following approximate equation for the coordination number

$$Z = Z_0 + c(R'/R - 1) \tag{14}$$

where $Z_0 = 7.3$ and $c = 15.5$. The necks which result from the original sphere contact points will be larger than the necks which form later. Taking this fact into account, Arzt has derived the following equation for the average contact area if all material remains in the necks:

$$a = 11(Z_0(R' - 1) + c(R' - 1)^2/2)R^2/ZR' \tag{15}$$

With this information, the first term of Equation 12, the effect of external pressure, may be evaluated.

Following Arzt, Ashby, and Easterling[6], the contact pressure due to surface tension is

$$p_s = \gamma\left(\frac{1}{w} - \frac{1}{x}\right) \tag{16}$$

where γ is the surface tension. The average neck area is known from Equation 15, so simple geometry will give the neck radius

$$x = \sqrt{a/\pi} \tag{17}$$

A reasonable approximation to the axial radius of curvature of the neck is given by

$$w = x^2/(2R - 2x). \tag{18}$$

This equation is not strictly consistent with Equation 15. Equation 15 describes a neck between two "overlapping" spheres like the one shown in Figure 13a: the material in the neck comes from the volume that the spheres would overlap if they were complete. Equation 18 describes the simpler geometry of Figure 13b for two "tangent" spheres: the material in the neck is supplied from some unspecified source. The inconsistency between these two approaches is judged to be insignificant for the following reasons: First, w affects only p_s, which will be shown later to be of secondary importance in determining p*. Second, p_s is uncertain since the surface tension is not well known. Third, both approaches assume a toroidal neck. Necks of this type are shown in the axial cross-sections of Figure 13: the profile of the neck surface is circular and tangent to both spheres. A toroidal neck is mathematically convenient, but this geometry would not be expected in a kinetic system. For these reasons, it is concluded that the expressions for w, x, and p_s are at best rather rough approximations.

The threshold contact pressure for motion of a grain boundary dislocation is also uncertain, since it depends on the Burgers vector of the dislocations and the type of dislocation sources. We have chosen to

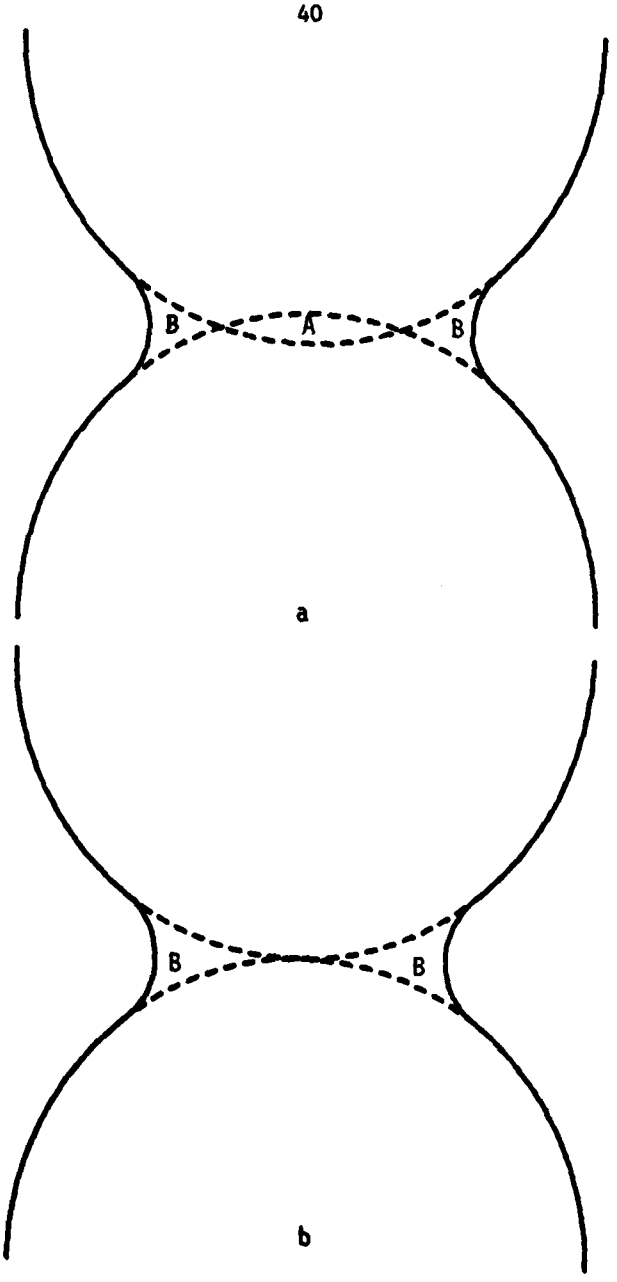

Figure 13. Two descriptions of neck geometry. a) The material in the neck comes from the spheres. The solids of revolution denoted by A and B-B have the same volumes. b) The material in the neck (B-B) comes from an unspecified source.

use the approach of Arzt, Ashby and Verrall. The threshold stress for grain boundary dislocation motion is

$$p_{th} = \frac{\sqrt{2}\ \alpha_o\ Gb_b}{x} \tag{19}$$

where $\alpha_o = 0.2$ is a constant which reflects the relative amount that the length of a dislocation must change in order to move.

As indicated in Equation 12, the effective contact pressure is the sum of three terms, which result from the externally applied pressure, surface tension, and the threshold stress for grain-boundary dislocation motion. Let us use the following data to calculate the magnitude of each of these effects. As suggested by SEM photographs of the fractured HIP specimens, let us use a particle radius R = 0.35E-6 m. A surface tension $\gamma = 1\ J/m^2$ is typical for ceramics. The data of Ryshkewitch[10] suggest the following equation for the shear modulus:

$$G = 12.382E9\ (1838.5-T)^{1/3}\ Pa \tag{20}$$

for temperatures less than 1600 K, where T is the temperature in kelvins. We have used a Burgers vector for lattice dislocations of b = 4.75E-10 m (for slip on the {0001} <1120> basal system)[11], and, following Arzt, Ashby, and Verrall[2], let $b_b = b/3$. Z_o, c, and α_o, as specified in Table 11.

Figure 14 shows the three terms of the effective contact pressure as functions of density. These curves were calculated for a temperature of 1150°C, but they depend only weakly on temperature. For the sake of completeness, the curves have been plotted over a density range from 0.65 to 0.995, even though the theory is not strictly valid over this entire range, as discussed below. The effect of surface tension is small relative to the effect of external pressure for all pressures considered. At low densities, the magnitude of the threshold pressure is comparable to the pressure due to surface tension. At a density of 0.70, an external applied pressure of 69 MPa (10000 psi) will produce a contact pressure of 507 MPa. Surface tension effects provide an additional 30 MPa of contact pressure, and the threshold pressure is 37 MPa,

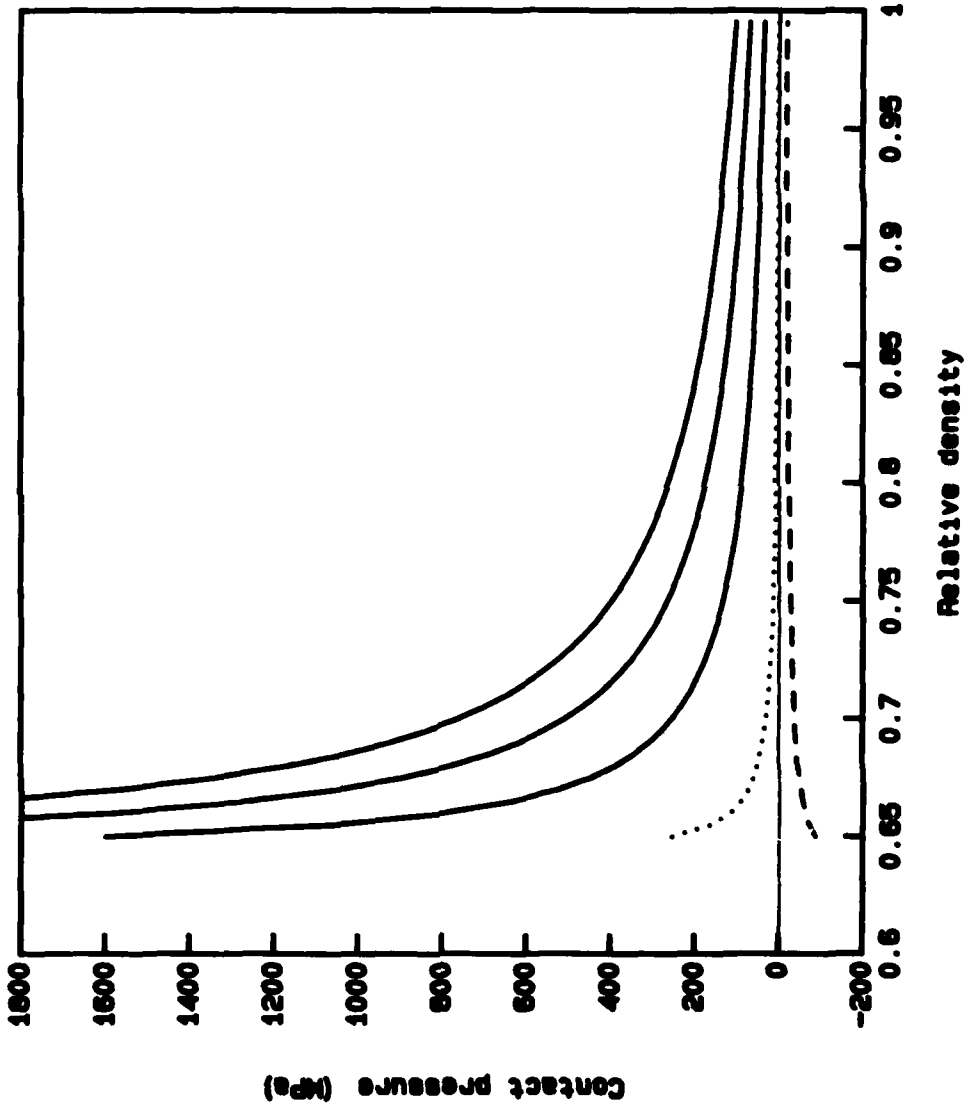

Figure 14. Contributions to the effective contact pressure from three sources as functions of density: external pressure (solid lines), surface tension (dotted line), and threshold for grain-boundary dislocation motion (dashed line). From bottom to top, curves for external pressure are for 34 MPa (5000 psi), 69 MPa (10000 psi), and 103 MPa (15000 psi).

so the effective contact pressure is 500 MPa. At high densities, the magnitude of the threshold pressure can be a significant fraction of the contact pressure due to the applied external pressure. Extending the previous example, at a density of 0.90, an external applied pressure of 69 MPa will produce a contact pressure of 99 MPa, surface tension effects will provide only 2 MPa of contact pressure, and the threshold pressure will be 20 MPa, producing an effective contact pressure of 81 MPa. If the external pressure is cut in half, the effective contact pressure drops to 32 MPa.

The total effective contact pressure due to all three terms is shown in Figure 15. For comparison, the bottom curve is drawn with no external pressure, corresponding to ordinary sintering. Note that the effective contact pressure crosses zero at a density near 0.69, predicting that sintering would stop at this density. This density will depend on the value chosen for the surface tension and the assumptions concerning neck geometry and threshold stress for dislocation motion. The theoretical prediction of limited sintering is supported by our work on sample preparation. Before HIP, the samples were sintered for 3 hours at 1100°C. The relative densities obtained were typically about 0.65; Table 8 lists the measured initial densities.

As an initial test, it is useful to ascertain that the theory does not require physically unrealistic values for any of its parameters. Combining Equations 5 to 7, 9, and 11, we may write

$$\frac{dD}{dt} = \frac{3D}{2R}\left(\frac{D}{D_o}\right)^{1/3}\left(\frac{b_n}{b_b}\right)^2 \frac{p^{*2} C_1 D_s \Omega}{G b_b \beta k T C_o} \qquad (21)$$

With the exception of D_s, rough estimates can be made of all of the variables in this equation. Following Arzt, Ashby, and Verrall, we may take $b_b = b/3$, $b_n = b_b/\sqrt{2}$, and $\beta = 10$. The value of Ω is unknown, since it is presently not known what solute might be responsible for controlling the motion of grain-boundary dislocations. However, a reasonable estimate is $\Omega = 2.15E\text{-}29\ m^3$, which is half of the volume of the formula unit. To compare theory with experiment, let us duplicate the conditions at one point in experiment 19. At an elapsed time of 269 minutes,

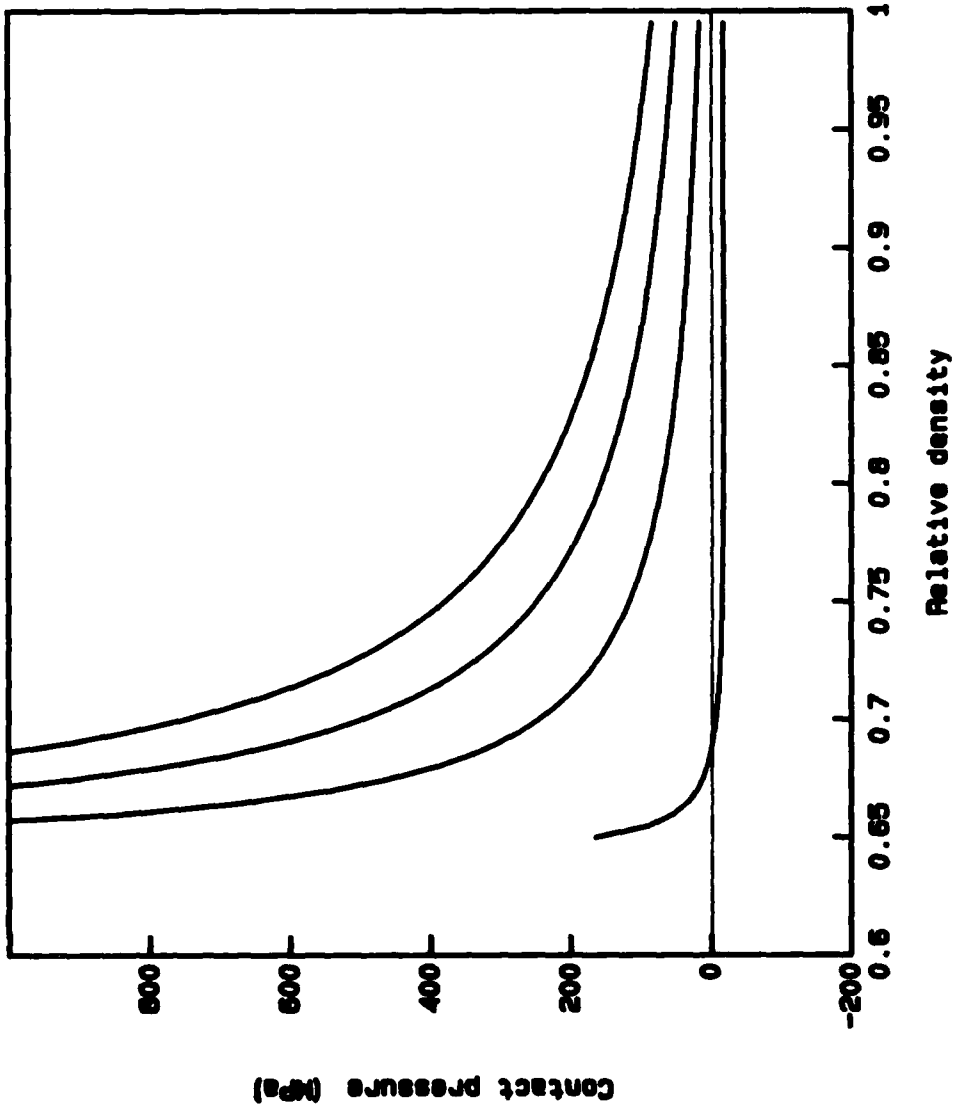

Figure 15. Total effective contact pressure as a function of density at various levels of applied external pressure. From bottom to top, curves for external pressure are for zero pressure, 34 MPa (5000 psi), 69 MPa (10000 psi), and 103 MPa (15000 psi).

we find that D = 0.8, T = 1273 K, p = 103 MPa, and the densification rate $dD/dt = 1.6E\text{-}5\ s^{-1}$. When all these values are substituted into Equation 21, we find that, for the theory to agree with the experiment, we must have $D_s = 1.2E\text{-}21\ m^2/s$. This is not an unreasonable diffusivity, so for this one piece of data, it has been shown that agreement between theory and experiment can be achieved with physically reasonable values for the parameters. It will be shown below that these parameter values are typical of those obtained by curve-fitting.

Although the controlling solute species is not known, it is possible to measure the activation energy for solute diffusion, E_s. By comparing the rates of densification at 1050°C and 1150°C, we obtained the values E_s = 316 kJ/mol for experiment 22a and E_s = 263 kJ/mol for experiment 22c, or an average value of 290 kJ/mol. Since some change in density occurred while the temperature was rising, a better value for E_s would be obtained if the measured densification rates were corrected for the density change. Unfortunately, a meaningful correction could not be made on the data for either experiment. In the case of experiment 22c, 1150°C was not reached until the probe indicated a density greater than 0.94. This density is well into the final stage, and we have not yet extended the theoretical model to the final stage. In experiment 22c, 1150°C was reached when the probe indicated a density of about 0.89, but, as discussed in the previous section, the calculated densities for this experiment are probably several percent below their actual values. Since the actual densities are not known, a reasonable correction for effect of density cannot be made. Since the change in density was small, however, the density correction is expected to have only a minor effect on the calculated activation energy.

An additional value of the activation energy, E_s = 419 kJ/mol, was obtained by comparing the data for experiments 19 and 20. This value is expected to be less accurate than those given above since it would be affected by any variations from sample to sample.

To compare the predictions of theory with the measurements of experiment, we have solved the differential equation for densification, Equation 21. A Runge-Kutta method[12] was used along with experimental records of external pressure and temperature as listed in Tables 2 to 7.

Linear interpolation was used between tabulated points. For the purposes of integration, it is convenient to recast Equation 21 as follows:

$$\frac{dD}{dt} = D\left(\frac{D}{D_o}\right)^{1/3} \frac{p^{*2}\exp(E_s/RT)}{GT}\, n \tag{22}$$

where R is the gas constant and n is given by

$$n = \frac{3}{2R}\left(\frac{b_n}{b_b}\right)^2 \frac{C_1 D_s^o \Omega}{b_b \beta k C_o} \tag{23}$$

In Equations 22 and 23, we have broken down the solute diffusivity using the standard Arrhenius equation

$$D_s = D_s^o \exp(-E_s/kT) \tag{24}$$

where D_s^o is the preexponential factor for the diffusivity of the solute and R is the gas constant. We have defined n so that it collects the parameters that were not determined by our experiments. Except for n, all the variables in Equation 22 have known values: the initial density D_o, the temperature T, and (through Equation 12) the effective contact pressure p* all come from the experimental data, the shear modulus G comes from the literature, and the activation energy for solute diffusion E_s was determined by experiment as discussed above.

We have used n as the single adjustable parameter in fitting Equation 22 to our data. It is appropriate to treat n as adjustable, since n contains several variables that have not been determined, such as b_b and Ω. We also used different values of n for different samples, so the theory has been applied to each experiment independently rather than to all six experiments as a group. This is also appropriate since n contains the preexponential factor for solute diffusion D_s^o, the solute concentration C_o, and the ratio of dislocation atmosphere concentration to bulk concentration β, all of which are probably subject to significant sample-to-sample variation.

The initial condition for Equation 22 is

$$D(t=0) = D_o. \tag{25}$$

This was the initial condition normally used in our integrations. In the integrations for experiments 22a and 22c, however, Equation 25 could not be used. When the density $D = D_r$, the geometrical description of the contacts between individual particles breaks down, predicting a zero contact area, $a = 0$. Equation 12 then gives an infinite effective contact pressure. For experiments 22a and 22c, $D_o < D_r$. It was therefore necessary to choose the initial condition so that $D(t=0) > D_r$, even if the measured initial density was lower than D_r. We chose to integrate with an initial density of 0.641.

The choice of the initial condition is relatively unimportant. This can be seen in Figure 16. Two integrations were performed using the temperature and pressure data for experiment 14. For one integration, the initial condition was as specified by Equation 25. For the second integration, we arbitrarily chose $D(t=0) = 0.70$. The same value of n was used in both cases. From Figure 16 it can be seen that even a relatively large change in the initial condition rapidly disappears at densification proceeds. The reason for this is straightforward. If temperature and external pressure are held constant, the densification rate decreases very strongly as the density increases from 0.64 to 0.7. It follows that a change in the initial density will largely disappear when significant densification begins.

Comparisons between data and experiment are shown in Figures 17 to 22. In these figures, the experimental density curves of Figures 2b to 7b are redisplayed along with theoretical density curves. The agreement between theory and experiment is evident. The values of n used for all of these calculations are relatively close, differing by at most a factor of 6. This is considered to be acceptable agreement. Since n is dependent on C_o, any variations between samples in the concentration of the rate-controlling solute will show up as a change in n. In addition, a change in the concentration of some other impurity may affect D_s^o or β, and thus change n.

All of the values for n correspond to physically reasonable choices of D_s, b_b, Ω, etc. This can be seen by a comparison with the sample calculation above. As has been argued, the values of the

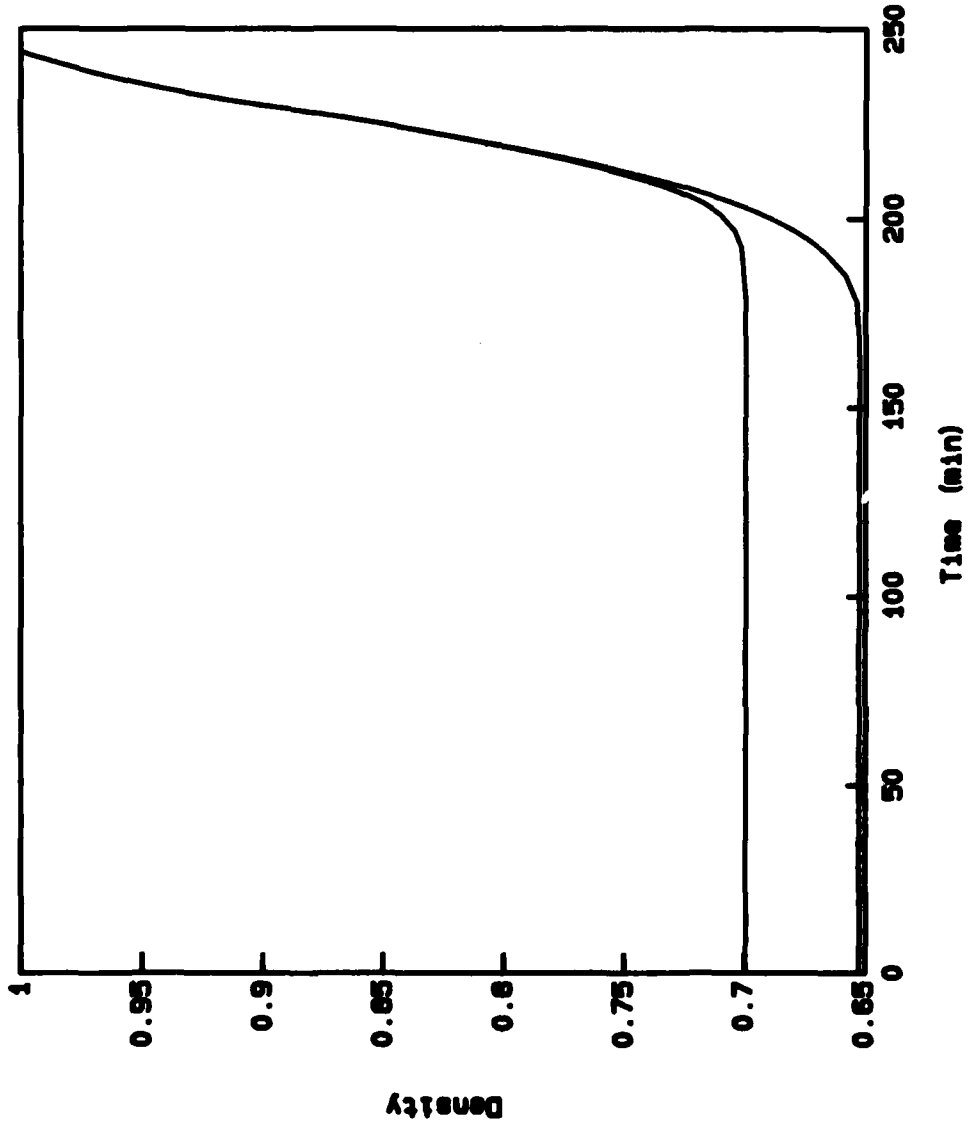

Figure 16. Effect of initial density on calculated density history. The dotted line was calculated with initial density 0.7, the dashed line with initial density 0.653. For both curves, n = 8E4. The temperature and pressure histories of experiment 14 were used.

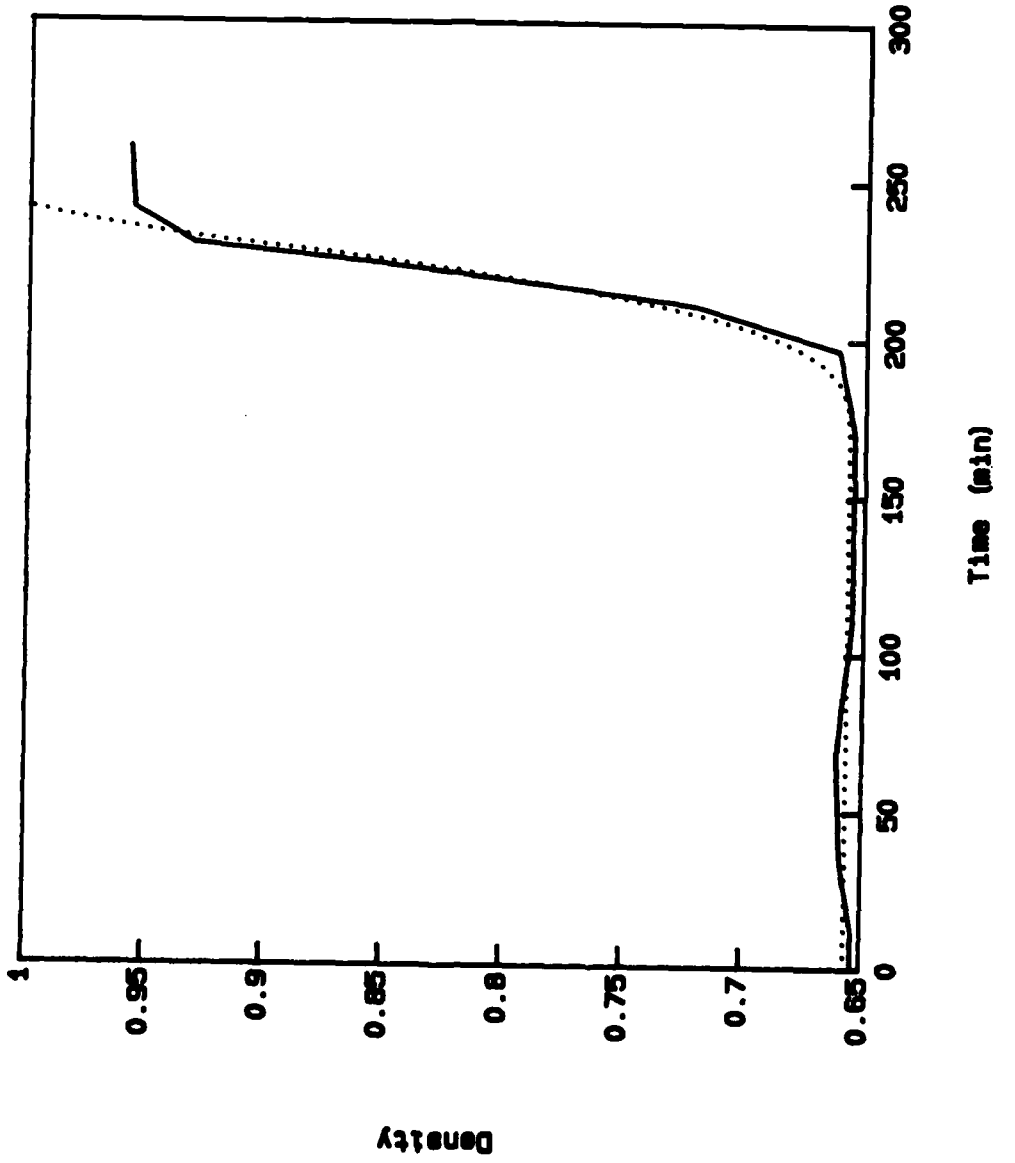

Figure 17. Comparison between experiment and theory for experiment 14. Solid line is experiment, dotted line is theory. Theoretical curve was calculated with n = 8E4.

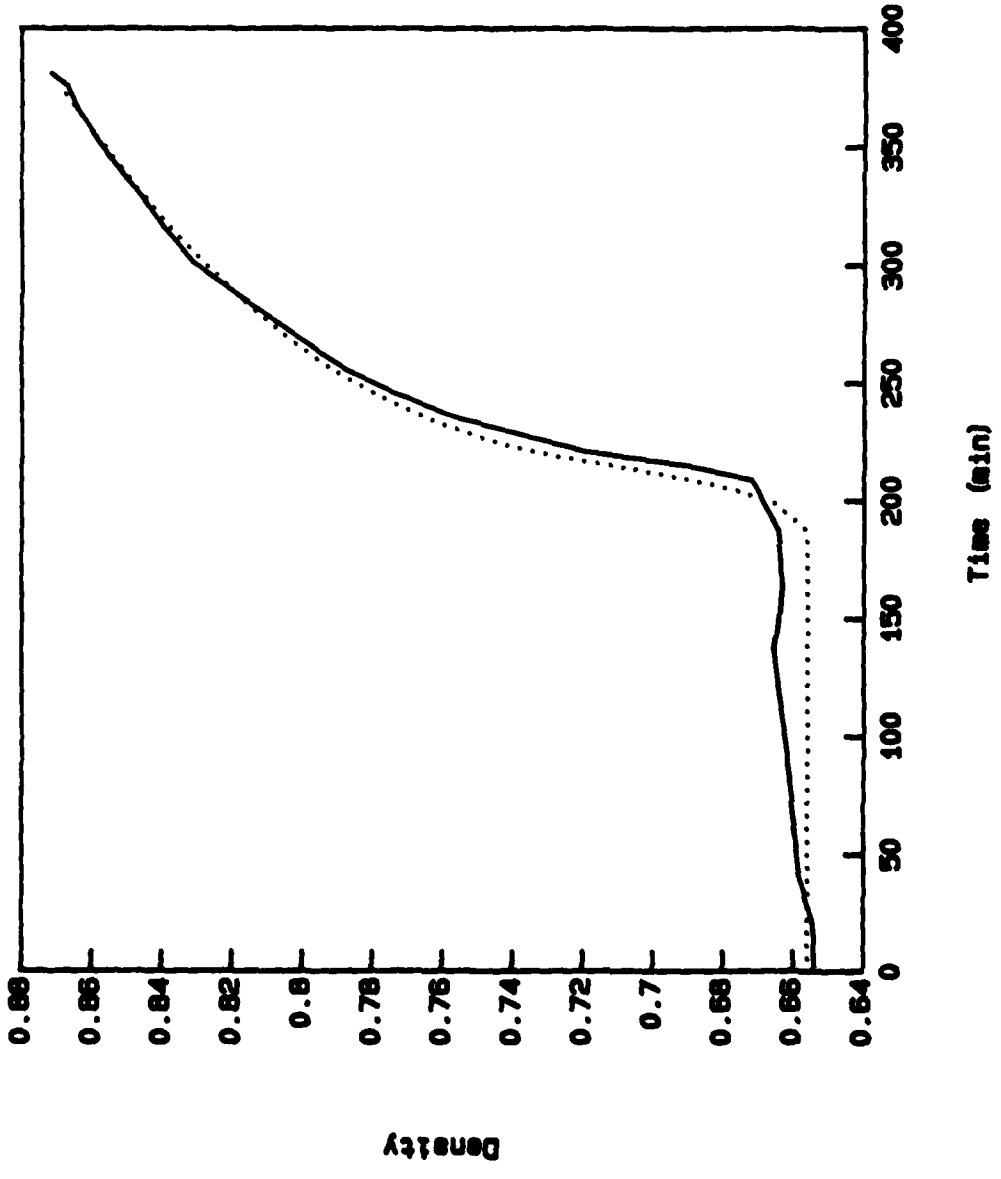

Figure 18. Comparison between experiment and theory for experiment 19. Solid line is experiment, dotted line is theory. Theoretical curve was calculated with n = 3.2E4.

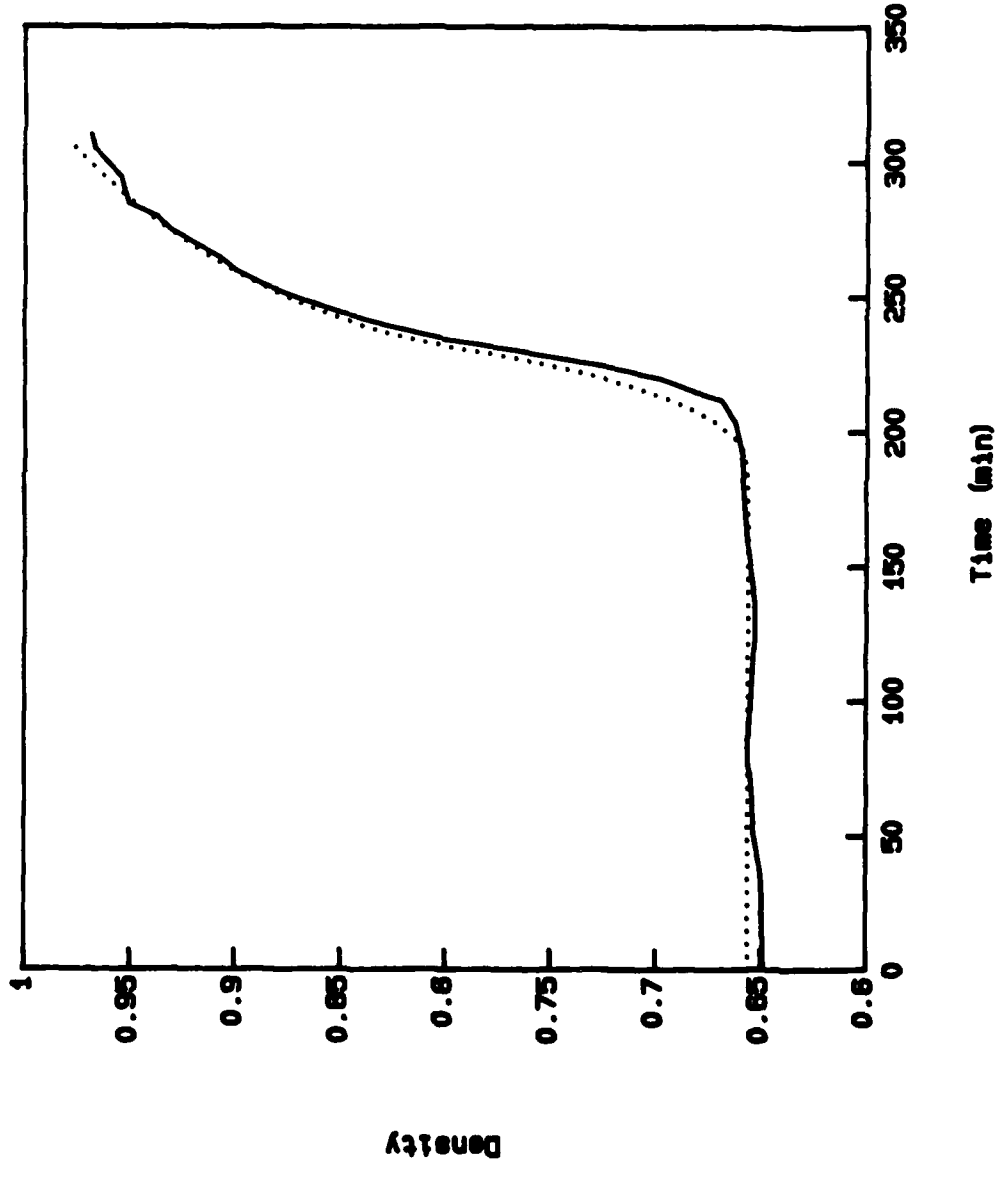

Figure 19. Comparison between experiment and theory for experiment 20. Solid line is experiment, dotted line is theory. Theoretical curve was calculated with n = 8E4.

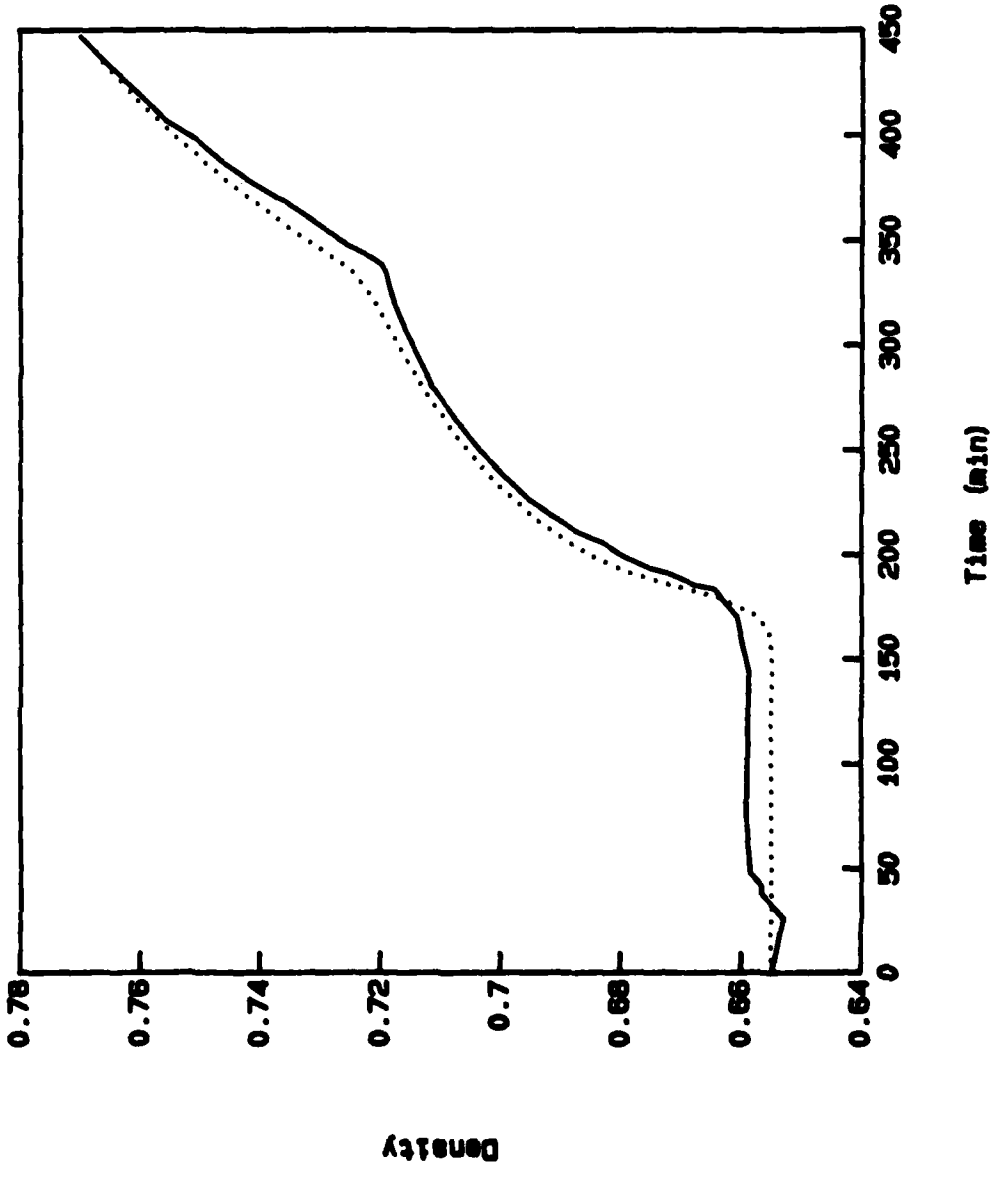

Figure 20. Comparison between experiment and theory for experiment 21. Solid line is experiment, dotted line is theory. Theoretical curve was calculated with n = 1.4E4.

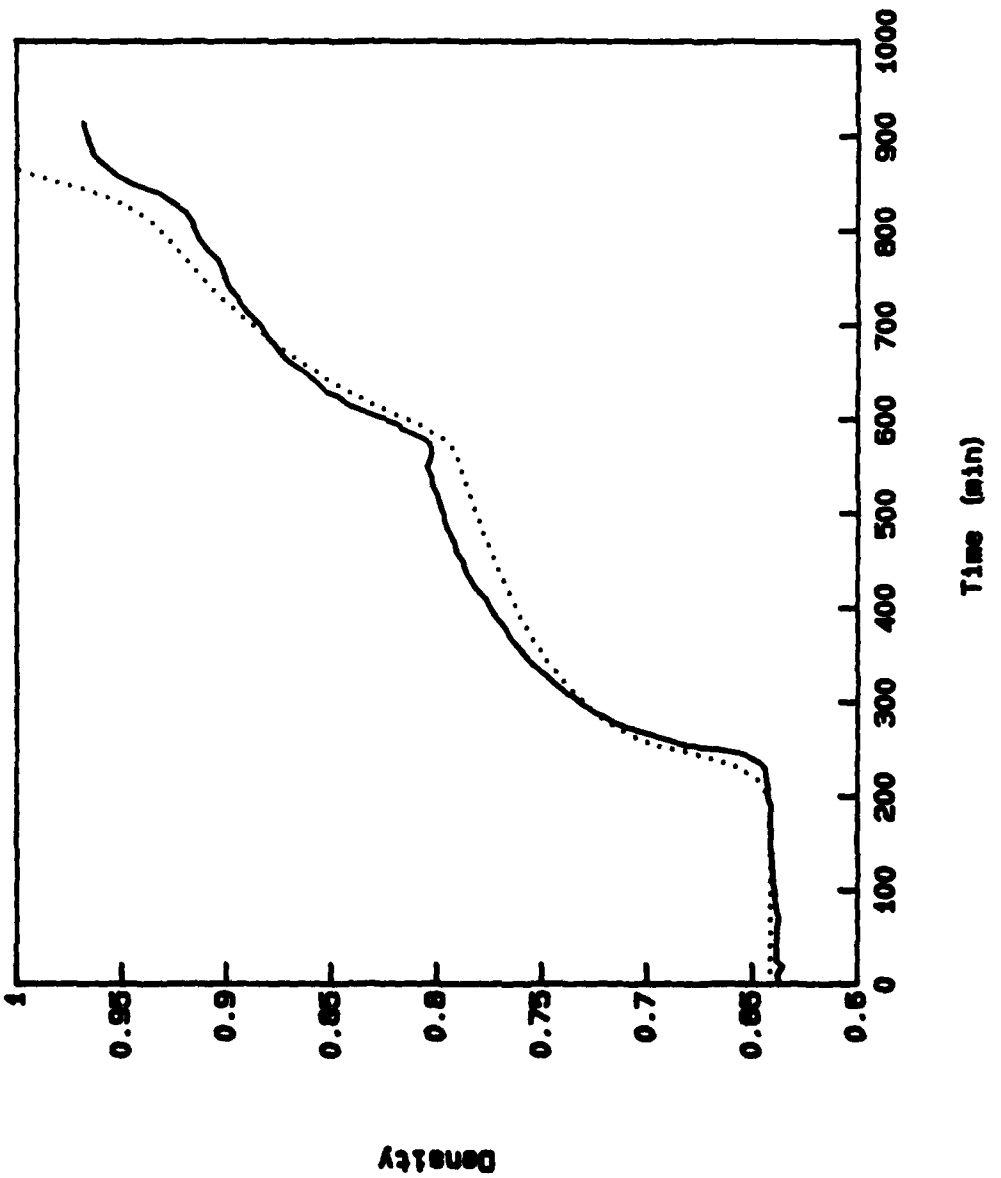

Figure 21. Comparison between experiment and theory for experiment 22a. Solid line is experiment, dotted line is theory. Theoretical curve was calculated with n = 1.8E4.

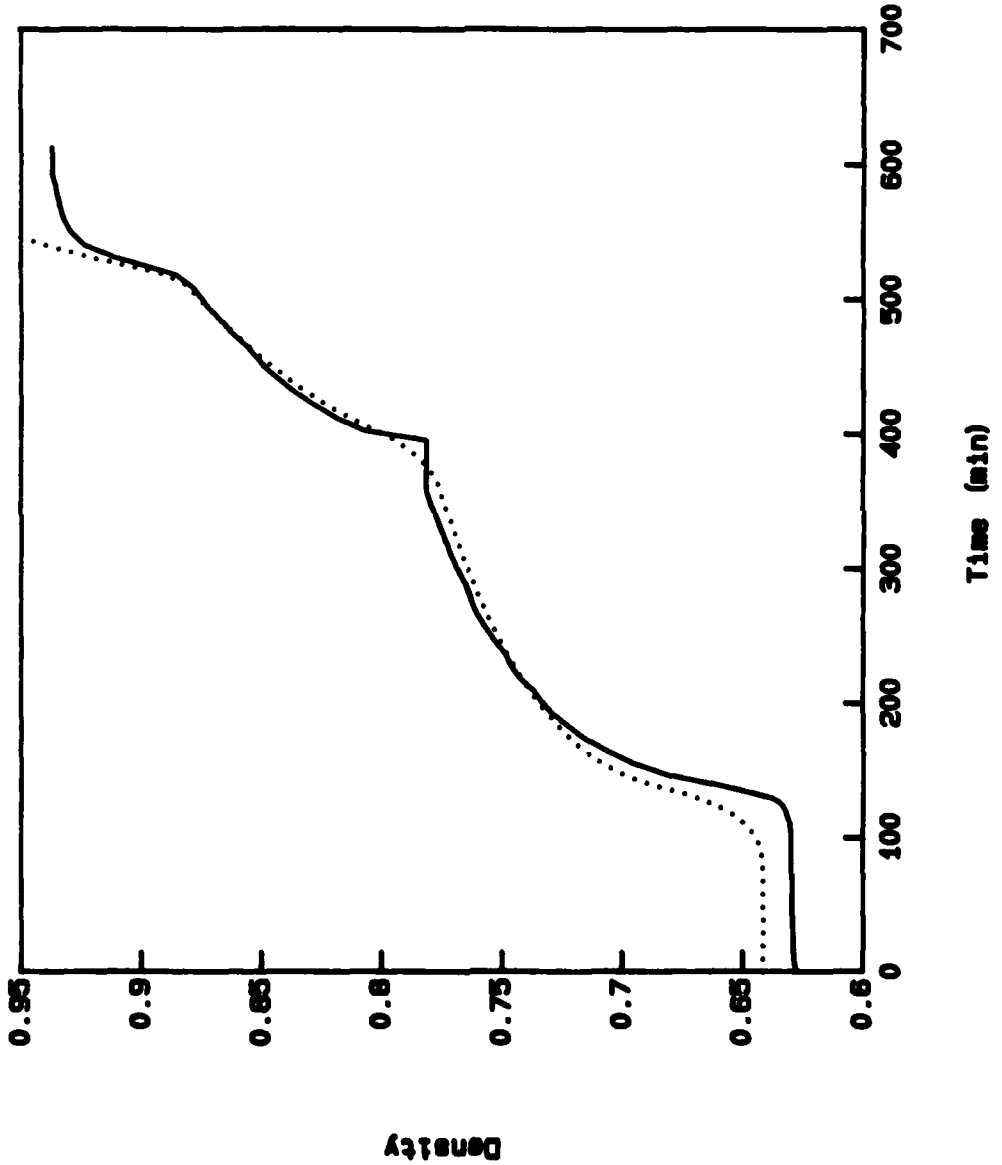

Figure 22. Comparison between experiment and theory for experiment 22c. Solid line is experiment, dotted line is theory. Theoretical curve was calculated with n = 1.6E4. Experimental density is not totally reliable for times between 361 and 396 minutes.

parameters used in the sample calculation are reasonable, and they correspond to n = 3.6E4. To provide the best description of all the data of experiment 19, we used n = 3.2E4. In either case, these values of n are typical of those obtained by curve-fitting for all of the six experiments, so the values of n used in the integrations also correspond to physically reasonable choices of the parameters.

A number of densification mechanisms have been discussed in the literature, including lattice and grain-boundary diffusion and climb and glide of dislocations. None of these mechanisms describes the results of our experiments as well as does the theory of interface-reaction controlled grain-boundary diffusion described above. A summary of the characteristics of each of these mechanisms is shown in Table 12. Values of activation energies for diffusion come from Mohamed and Langdon[13]. All of the diffusional mechanisms fail in that they do not predict the correct dependence of densification rate on pressure. Studies of data for experiments 21, 22a, and 22c indicate that densification rate varies like p^m where p is the external pressure and the pressure exponent m is between 2 and 2.2. By contrast, the diffusion-controlled mechanisms all predict a pressure exponent of 1. The dislocation mechanisms also fail, although they predict a pressure dependence which is stronger than that of interface-controlled diffusion. There is also no notable agreement on activation energies, although the energies for grain-boundary diffusion are moderately close. The activation energy for dislocation climb is too high. The activation energy for dislocation glide depends on the slip system, but at the temperatures used in our experiments (1000 to 1150°C) only the basal slip system is active, so slip could contribute only a small amount of densification. The most logical explanation of the data, therefore, is that densification occurs by interface-reaction controlled grain-boundary diffusion.

As it presently stands, the theory described above would be expected to break down outside the density range 0.65 to 0.9. At densities below D_p, the picture of a random dense packing is inadequate to explain the density, and the structure of an aggregated or agglomerated powder becomes important. Densification of an agglomerated powder would

TABLE 12. COMPARISON OF VARIOUS MECHANISMS FOR DENSIFICATION

Mechanism	Pressure Exponent	Activation Energy (kJ/mol)
Lattice Diffusion		
Al Control	1	478
O Control	1	637
Grain Boundary Diffusion		
Al Control	1	419
O Control	1	226
Dislocation Climb	~ 3	637
Dislocation Glide	~ 5	?
Interface-Reaction-Controlled Diffusion	2	?
Experiment	2.1	290

be difficult to model, but it also appears that it is unnecessary to model it since HIP would tend to break down the agglomerates. When the density is only slightly above D_p, the theory is subject to doubt because it predicts extremely high effective contact pressures. At high densities, the primary difficulties appear to be geometrical. Perhaps the most important effect is that the pores begin to close, typically at a density near 0.9, and a completely new description of the pore geometry is needed. It should be noted, however, that the theory is in good agreement with experiment to densities as high as 0.95. From an empirical point of view, the model is useful in the density range 0.9 to 0.95 even if its theoretical justification is doubtful. To overcome these difficulties, we currently plan to extend the model to the final stage in the coming year.

PUBLICATIONS AND PRESENTATIONS

Publications and Presentations that have arisen from this research to date are:

1. J.K. McCoy, "A Rational Method for Calculating Mechanism Maps", Scripta Met. 17 563-568, 1983.

2. R.R. Wills and J.K. McCoy, "HIP of Al_2O_3: Theory versus Experiment", Basic Science Division of the American Ceramic Society, Spring Meeting, Pittsburgh, PA, May, 1984.

3. J.K. McCoy, "A Coherent Method for Calculating Mechanism Maps", Basic Science Division of the American Ceramic Society, Fall Meeting, Columbus, Ohio, November, 1983.

4. R.R. Wills and J.K. McCoy, "Hot Isostatic Pressing Densification Maps", Basic Science Division of the American Ceramic Society, Fall Meeting, Columbus, Ohio, November, 1983.

ACKNOWLEDGMENTS

The authors would like to thank Mr. L.E. Muttart for preparing the specimens, Mr. R. Palmer for performing the HIP experiments, and Dr. Alan Markworth for his technical comments and suggestions.

REFERENCES

1. Y. S. Touloukian, Thermophysical Properties of High Temperature Solid Materials, vol. 3, pp. 211-212, vol. 4, pp. 22-25, Macmillan, New York, 1967.

2. E. Arzt, M. F. Ashby, and R. A. Verrall, "Interface Controlled Diffusional Creep", Acta Met. 31 1977-1989 (1983)

3. A. H. Cottrell and M. A. Jaswon, "Distribution of Solute Atoms Around a Slow Dislocation", Proc. Roy. Soc A199 104-114 (1949)

4. A. H. Cottrell, Dislocations and Plastic Flow in Crystals, Oxford, 1953.

5. B. Burton, "Interface Reaction Controlled Diffusional Creep: A Consideration of Grain Boundary Dislocation Climb Sources", Mat. Sci. Eng. 10 9-14 (1972)

6. E. Arzt, M. F. Ashby, and K. E. Easterling, "Practical Applications of Hot-Isostatic Pressing Diagrams: Four Case Studies", Met. Trans. A 14 211-221 (1983)

7. E. Arzt, "The Influence of an Increasing Particle Coordination on the Densification of Spherical Powders", Acta Met. 30 1883-1890 (1982)

8. G. D. Scott, "Radial Distribution of the Random Close Packing of Equal Spheres", Nature 194 956-958 (1962)

9. G. Mason, "Radial Distribution Functions from Small Packings of Spheres", Nature 217 733-735 (1968)

10. E. Ryshkewitch, "Rigidity Modulus of Some Pure Oxide Bodies - 8th Communication to Ceramography", J. Am. Ceram Soc. 34 322-326 (1951)

11. T. G. Langdon and F. A. Mohamed, "Deformation Mechanism Maps for Ceramics", J. Mat. Sci. 11 317-327 (1976)

12. G. Dahlquist and A. Bjorck, Numerical Methods, p. 346, Prentice-Hall, Englewood Cliffs, New Jersey, 1974.

13. F. A. Mohamed and T. G. Langdon, "Recent Development in Deformation Mechanism Maps for Ceramics", in Ceramic Microstructures '76, pp. 763-773, ed. R. M. Fulrath and J. A. Pask, Westview, Boulder, Colorado, 1976.

APPENDIX

The following pages contain a listing of a Fortran program to convert measurements of can shrinkage into relative densities, given the initial can geometry. The program includes correction for thermal expansion and thickening of the can wall.

```
      program probdens
c
c     This program converts probe readings and temperatures to sample
c     densities.
c
c
c     key to variable names
c     l = length
c     d = diameter (outside)
c     w = wall thickness
c
      real l init sample, l finl sample, l init can,
&     l finl can, l init plugs, l finl plugs
      common /sizes/ l init sample, l finl sample, l init can,
&     l finl can, l init plugs, l finl plugs, d init sample,
&     d finl sample, d init can, d finl can, w init can,
&     w finl can, density init, alpha
      character*20 text
c
c     time is in minutes
c     pressure is in psi
c     temperature is in centigrade
c     probe reading is in (negative) mils
c             (positive probe reading <=> shrinkage)
c             (negative probe reading <=> expansion)
c
c     dimensions in /sizes/ are in inches or cubic inches
c     alpha and density init are dimensionless
c
      open(unit=7,file='canout',status='unknown')
      open(unit=5,status='old')
      rewind(5)
c
c     read sample dimensions
      call readsize
c
c     read off heading lines
      read(5,'()')
      read(5,'(a20)') text
5     read(5,50010,end=20) time, pressure, temperature c, probe
50010 format(5x,f7.1,f7.0,f6.0,f9.0)
      write(6,6001) time, pressure, temperature c, probe
6001  format(5x,f5.1,f7.1,f6.1,f9.2)
      temperature=temperature c+273.
c
c     Correct for initial can size.
c     (d can is diameter of can at current temperature.)
c
```

```
      d can=d init can-probe/1000.
c
c     Find upper and lower limits of physical probe readings.
c
      density min=.6
      density max=1.
      call densprob(d can max,density min,temperature)
      call densprob(d can min,density max,temperature)
      if(d can.gt.d can max) then
        write(6,'('' probe reading too large.'')')
        go to 5
      else if(d can.lt.d can min) then
        write(6,'('' probe reading too small.'')')
        go to 5
      end if
c
c     Calculate density.
c
      iapprox=0
10    density apx=density min+(density max-density min)*
&           ((d can max-d can)/(d can max-d can min))
      call densprob(d can apx,density apx,temperature)
      iapprox=iapprox+1
      if(d can apx.ge.d can) then
        d can max=d can apx
        density min=density apx
      else if(d can apx.le.d can) then
        d can min=d can apx
        density max=density apx
      end if
      if((density max-density min.gt.1.e-5).and.iapprox.lt.12) go to 10
      write(7,60010) time, temperature c, pressure, probe, density apx
      write(6,60010) time, temperature c, pressure, probe, density apx
60010 format(f8.2,2f8.0,f8.2,f9.4)
      go to 5
   20 stop
      end
      subroutine densprob(d can,density,temperature)

c     This routine calculates can diameter for a given density.
c
      real l init sample, l finl sample, l init can,
&     l finl can, l init plugs, l finl plugs
      common /sizes/ l init sample, l finl sample, l init can,
&     l finl can, l init plugs, l finl plugs, d init sample,
&     d finl sample, d init can, d finl can, w init can,
&     w finl can, density init, alpha
c
```

```
      real l sample,l sample init, l sample init 20
      data pi/3.1415926/
c
      l sample init 20=l init sample
      volume init 20=pi*l init sample*d init sample*d init sample/4.
      d sample init 20=d init sample
      vol can 20=(l finl can - l finl plugs)*pi*
     &  (d finl sample + w finl can)*w finl can
c
c     Calculate integrated thermal expansion.
c
      expand al2o3=7.2978e-6*(temperature-293.)+
     &       7.8486e-10*(temperature-293.)*(temperature-800.)
      expand 304ss=1.7751e-5*(temperature-293.)+
     &       5.0423e-9*(temperature-293.)*(temperature-800.)
c
c     Correct lengths and volumes for temperature.
c
      d sample init=d sample init 20*(1.+expand al2o3)
      l sample init=l sample init 20*(1.+expand al2o3)
      volume init=volume init 20*(1.+3.*expand al2o3)
      vol can=vol can 20*(1.+3.*expand 304ss)
c
c     Calculate can geometry.
c
      volume=volume init*(density init/density)
      d sample=((4*volume*d sample init**alpha)/(pi*l sample init))**
     &       (1./(2.+alpha))
      l sample=(4.*volume)/(pi*d sample**2)
      wall=(-pi*l sample*d sample+
     &       sqrt((pi*l sample*d sample)**2+4.*pi*l sample*vol can))
     &       /(2.*pi*l sample)
      d can=d sample+2.*wall
      return
      end
      subroutine readsize
c
c     this routine reads size dat for the sample
c
      real l init sample, l finl sample, l init can,
     &  l finl can, l init plugs, l finl plugs
      common /sizes/ l init sample, l finl sample, l init can,
     &  l finl can, l init plugs, l finl plugs, d init sample,
     &  d finl sample, d init can, d finl can, w init can,
     &  w finl can, density init, alpha
c
      read (5,505) l init sample, l init can,
     &  l finl can, l init plugs, l finl plugs, d init sample,
```

```
&       d init can, d finl can, w init can,
&       w finl can, density init
505     format (f6.0)
c
        l finl sample=l finl can-l finl plugs
        d finl sample=d finl can-2.*w finl can
        alpha=log(l finl sample/l init sample)/
&       log(d finl sample/d init sample)
        return
        end
```

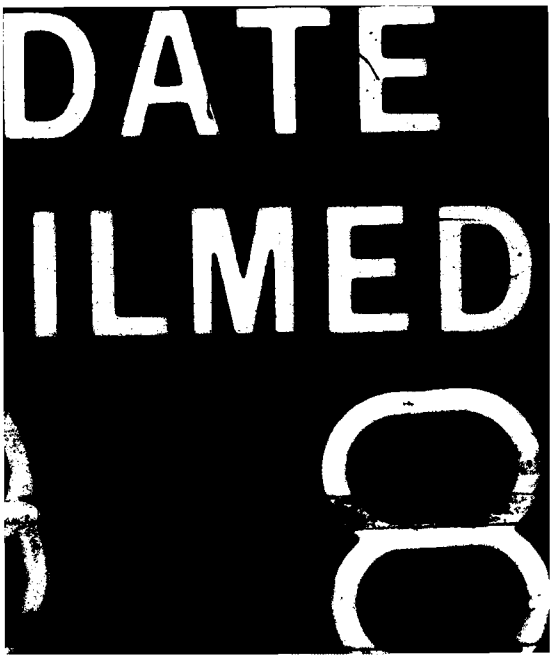
DATE
ILMED